Water content estimation of seasonal snow derived from subsurface temperature measurements at Finse, Norway

Ørjan Søderblom

Thesis submitted for the degree of
Master in Physical geography
60 credits

Department of Geosciences/
Mathematics and Natural sciences

UNIVERSITY OF OSLO

June 2019

Water content estimation of seasonal snow derived from subsurface temperature measurements at Finse, Norway

Ørjan Søderblom

2019

Water content estimation of seasonal snow derived from subsurface temperature measurements at Finse, Norway

Ørjan Søderblom

http://www.duo.uio.no

Trykk: Reprosentralen, Universitetet i Oslo

Cover photo by the author.

Abstract

Finse is an alpine mountain region situated in the northern part of Hardangervidda, in the central part of southern Norway. As a result of its high-altitude location over 1200m above sea level, Finse experiences near continuous snow cover between the months of November and the end of May. Over the winter of 2017/2018 and 2018/2019 the area had a winter mean temperature of -1,5° C and 0,1° C respectively.

Over the two winter seasons of 2017/2018 and 2018/2019, field work and observations of subsurface temperatures by thermistorstring were developed and used to monitor temperature changes within the snowpack. The aim of this was to simulate the temperature evolution and calculate refreezing capacities of the observed and simulated snowpack. The difference in refreezing capacities represent the amount of water that has refrozen within the snow.

The instruments built for this thesis gave promising results and it was concluded the use of thermistorstrings provide a good way to measure snow temperature non-invasively. The input parameters density, effective thermal conductivity and heat capacity were chosen to optimize the model. The model does not include realistic input parameter values, as they are chosen to optimize the simulation in cold snow. The water content estimation of 2017/2018 resulted in a value of 1,72 kg m^{-2} in the end of the data period.

Acknowledgments

This thesis is the final work of my master's degree in physical geography at the University of Oslo, department of geosciences.

I would like to thank the Finse field group for superb company and cooperation during field work, with a special thanks to Simon Filhol and John Hult for all the help and problem solving.

I also like to thank my main supervisor Thomas Vikhamar Schuler and my co-supervisor Karsten Müller.

Thanks also appointed to all my classmates during the years for interesting discussions and valuable laughs.

Blindern, June 2019

Ørjan Sødeblom

Table of contents

Figures and tables

1 Introduction

1.1 Motivation

Studying snow is of importance for several reasons and interests, such as avalanche forecasting, flood forecasting, water resource estimation for the hydropower industry and mass balance calculations on glaciers. It also plays a key role in our global climate with its immense ability of cooling (Sturm, Goldstein et al. 2017). About one sixth of the world's population relies on water from snowmelt for both human consumption and agriculture (Barnett, Adam et al. 2005). Sturm, Goldstein et al. (2017) researched the financial value of snow, and from that calculations gave an indication of an order in the trillions of dollars.

1.2 Objective

The objective of this work is to develop thermistorstring for non-invasive, subsurface temperature measurements of the seasonal snow at Finse during the two winter seasons of 2017/2018 and 2018/2019. This will be done using temperature measurements to estimate the water content of the snowpack by considering the difference in refreezing capacity of observed and simulated temperature. From this estimated parameter, the amount of refrozen water in the snowpack can be derived. The work is supported by snow pit observations. In addition, near infrared photography will be tested as an objective validation tool for observing snow layering.

1.3 Structure

The thesis is divided into sections, starting with a background of relevant topics in chapter 2. Chapter 3 describes the methods used for building the instrument and what values are used for the model. Chapter 3 also includes a description of the model and the calculation of water content. Chapter 4 gives results before chapter 5 discusses results. Finally, a conclusion and improvement suggestions in chapter 6.

2 Background

2.1 Snow

Snow as precipitation is formed in clouds at temperatures below the freezing point. The clouds need to consist of supercooled water droplets that condensate and freeze on nuclei in the sky. Because of the difference in saturation vapor pressure between ice and water, the newly frozen water droplet quickly grows at the expense of remaining water droplets. The form of the snow crystal depends on temperature and supersaturation in the clouds (Armstrong and Brun 2008).

Snow is deposited as a sediment, but often re-deposited by aeolian re-deposition. As deposited sediment, the snow then becomes a monomineralic rock consisting of ice. The snowpack can have a broad range of density, from 50 to 550 kg m^{-3}. The snow undergoes metamorphism, both close-to-surface metamorphism (mechanical) and internal metamorphism. The temperature of snow is very high and close to its melting point. The homologous temperature ($T_H = \frac{T(K)}{T_{mp}(K)}$) of snow is around 0,9 meaning it is very close to its melting temperature (Schneebeli 2002).

2.2 Snowpack metamorphism

Snow crystals goes through changes over time as it becomes part of the snowpack. These changes may happen rapidly, or over a longer time period. The large surface to volume ratio of a snow crystal makes it quite unstable for transformations. The changes in the snow is important to have knowledge of, as it influences the snowpack density and structure, and hence other physical processes within the snowpack. The metamorphic processes that causes transformations are divided into two main groups of dry and wet snow metamorphism.

2.2.1 Dry snow metamorphism

There are two types of metamorphism in dry snow, constructive and destructive, also known as respectively kinetic growth form and equilibrium growth form metamorphism.

Equilibrium form

Vapor diffusion over crystal surfaces, also called equilibrium-temperature metamorphism. It is driven by differences in vapor pressure between convex and concave ice surfaces, hence

sublimation of water vapor from edges to depressions on individual snow crystals. This decreases the crystal surface and the effect of this is formation of rounded, well-bonded ice grains (DeWalle and Rango 2008). The equilibrium form growth is temperature dependant and the process slow down with decreasing temperatures.

Kinetic growth form (temperature-gradient metamorphism)

Kinetic growth form is vapor diffusion among crystal that is driven by temperature gradients in the snowpack. The physical principle is that the water vapor diffuses from places with higher water vapor pressure (warmer temperatures) to places with lower water vapor pressure (colder temperatures), typically from the lower parts of the snowpack towards the atmosphere. As a general assumption it is expected to be close to 0° C at the snow/ground transition because of geothermal heat as well as heat stored in the ground during summer. The warmer air consists of more water vapor and has a higher water vapor pressure than air higher up within the snowpack. The differences in water vapor pressure leads to a transport of vapor towards areas with less vapor pressure. As the water vapor is transported in the direction of the pressure gradient, it cools down and condensates on other snow crystals. There are three determining factors on the rate of growth and which crystal type that forms:

- Temperature
- Temperature gradient
- Size of pore space

At high temperature and large pore space, the rate of growth is at its highest and conditions are favourable for depth hoar growth. The temperature gradient considered as threshold for kinetic growth is 10° C/m or more (McClung and Schaerer 2006).

2.2.2 Wet snow metamorphism

Wet snow metamorphism occurs if the snowpack is subjected to any kind of liquid water. If there is liquid water present, the temperature is 0° C. The water vapor pressure is depending on the curvature of the respective grain as well as that the vapor pressure is higher over water than ice. This gives the larger grain a higher melting temperature than a smaller. Consequently, this causes the smaller grains to melt while the larger grow on their behalf (McClung and Schaerer 2006, DeWalle and Rango 2008).

Pressure

In the occasions where snow doesn't melt for years, and becomes perennial, slow compression causes a visco-elastic deformation of the ice-grains. The process is driven by new snow on top of the old, which leads to firn and eventually glacial ice (DeWalle and Rango 2008).

2.3 Temperature gradient

The snowpack is situated in the cross section between the ground and the atmosphere, and the temperature within the snow is determined by the conditions at both sides. The heat stored in the ground during summer, as well as the geothermal heat from the earth's core, leads to a temperature at the snow base of, or close to, 0° C. The upper part is affected by the air temperature, which can vary several degrees from day to day, and also from daytime to night-time. Due to this difference, a temperature gradient is present for the vast majority of the winter season. The temperature gradient is defined as the change in temperature (ΔT) divided by the distance (Δx), and the direction of the vector is by convection in the direction of increasing temperature. A temperature gradient of 0° C/m implies an isothermal snowpack, which based on general assumptions implies a wet snowpack throughout (McClung and Schaerer 2006).

The temperature gradient is a major factor in snow metamorphism, as it has a direct correlation to the water vapor pressure gradient (Colbeck 1982). The strength of the temperature gradient is determining which metamorphic processes that is expected in the snowpack, and because it is a property that requires little effort to measure.

2.4 Water in snow

When water infiltrates a cold snowpack it will start filling the pore space initially filled with air. The infiltrated water will refreeze and release latent heat of fusion in response. This process heats the snow, and as melt or rain continues it can heat even deep snowpacks rather quickly if conditions are favourable. All added water is obtained within the snow until the temperature reaches isothermal 0° C, at least in drainage channels going from top to bottom (DeWalle and Rango 2008).

Conway and Benedict (1994) did experiments on rain on snow events, and by measuring temperature in a grid in the snowpack they could monitor the wetting process. The snowpack in the first event consisted of two crust layers at different depths and other than that fine-grained snow in general. They observed a pattern they call "step and fill", referring to the ponding and lateral flow of water as the wetting front reaches the crust layers. In the first event it took around four hours before the first crusts were penetrated, and at this time all of the snow above had been wetted. They observed the same pattern at the next crust with lateral flow, but here the water did not penetrate further before the precipitation ceased. Above both the first and the second crust layer, there were areas in the snow that reached 0° C before adjacent thermistors, a sign of finger flow.

2.4.1 Cold content

The cold content is the value on the amount of liquid water from melt or rain that needs to refreeze within the snowpack to heat it from current temperature to an isothermal 0° C. All added water is obtained within the snow until the temperature reaches isothermal 0° C, at least in drainage channels going from top to bottom. The cold content is important to help determining the timing of outflow, by comparing to forecasted rainfall or expected melt events. The daily temperature fluctuations must be considered, as night temperatures are often considerably lower than during daytime (DeWalle and Rango 2008). In this work the cold content will be mentioned as refreezing capacity (RC) (Marchenko, van Pelt et al. 2018).

2.4.2 Driving forces

Earlier theories of water movement in snow were based on corresponding theories of water movement in other sub surface materials such as gravitational flow. What makes the process in snow more difficult is that snow undergoes rapid changes as it interacts with liquid water. The snow properties tend to change significantly as grains grow, density increases and ice/crust layers decompose (Colbeck 1979). The capillary gradients in snow were usually

neglected in early theories, so refreezing and ice layers were thought to be the main cause of heterogeneous water movement (Hirashima, Avanzi et al. 2017). Observations by Avanzi, Hirashima et al. (2016) of water infiltration in layered snow revealed that capillary barriers and preferential flow are relevant processes controlling the speed of infiltration. They also state that grain size affects the spatial variability of water transmission, as it increases in a coarser grained medium. One of the experiments by Avanzi, Hirashima et al. (2016) confirm that a finer-over- coarser snow texture is subjected to ponding of water and horizontal spread at the textural transition. This is because the infiltrating water generally has a very high suction when it initially moves in the finer layer, leading to ponding of water within this layer as it is prevented from entering lower layers. This is often referred to as 'capillary barriers', and the capillary forces increase the finer the snow is. The preferential flow seems to be the dominant process in water transmission in snow. The snow in these flow paths, or fingers, went through grain growth as response to wet snow metamorphism.
In addition to capillary barriers, ice layers and crusts with low permeability, also prevents water infiltration. Before these layers have undergone the thermodynamic disintegration, ponding of water and lateral dispersion will occur. When the ice or crust layers have been exposed to a sufficient amount of energy by the liquid water, small drainage holes give a basis for finger flow (Colbeck 1979).

2.4.3 Flow patterns

When water flows down in a snowpack and reaches pre-melted stratigraphic horizons it normally will pond here (Marsh and Woo 1984). As mentioned earlier, Colbeck (1979) discusses the further development of finger flow into the lower stratum. This type of finger flow may occur down through the whole snowpack, depending on the layer properties following further down. This flow process allows only parts of the snow to be warmed by release of latent heat from refreezing; hence a large portion of the snow still have potential of being sub-freezing (Conway and Benedict 1992). Figure 1 shows finger flow within the snowpack in an experiment by Marsh and Woo (1984), and we can clearly see the lateral spread and ponding of dyed water at stratigraphic horizons, as well as the vertical flow paths, which constitutes finger flow.

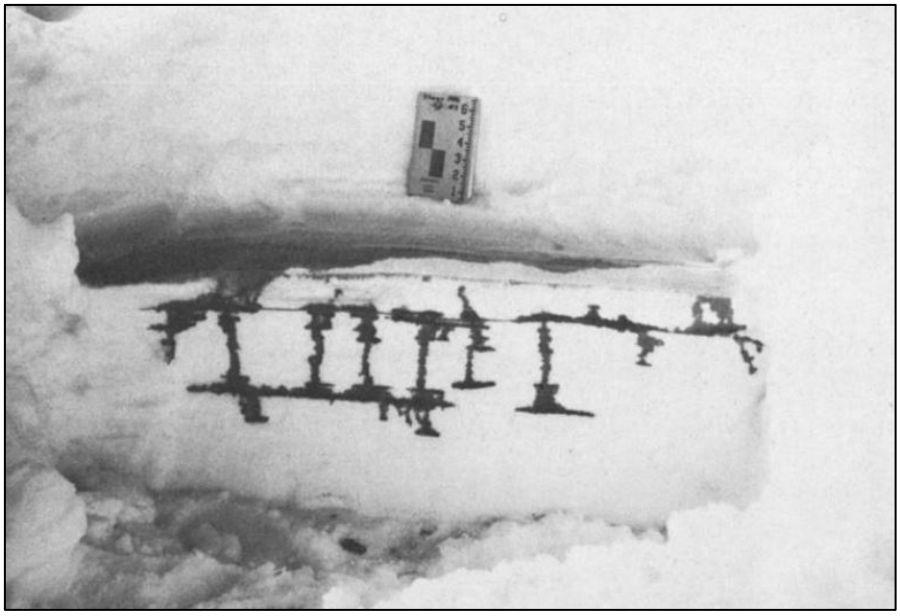

Figure 1: An example of finger flow within a heterogeneous snowpack, presented by a profile wall (Marsh and Woo 1984).

In later melt or rain events these fingers will most likely be the preferential flow paths, as they already have undergone wet snow metamorphism and therefore also have increased grain size (Marsh and Woo 1984). When the flow paths reach the ground or other surfaces that drains the water (DeWalle and Rango 2008), and as this process matures, flow channels form. The flow channels are bigger than the fingers and reaches from snow surface to drainage surface. Figure 2 is a picture of what a set of very mature drainage channels may look like. In this case the snowpack had been exposed to quite heavy rain for several days, and we can clearly see the wavy structure with the drainage channels in the depressions.

Figure 2: Picture of well-developed melt channels on snow surface after a period of rain (picture: Ørjan Søderblom).

2.4.4 Snow stability during rain/melt event

As water percolates the snow and the wet snow metamorphism happens, the grain growth and its subsequent changes in pore sizes and distribution under wet snow conditions decrease snow strength which can lead to wet snow avalanches (Brun 1989, Mitterer and Schweizer 2013). The stability of a rain or melt on snow event is changing through roughly three steps. First the initial, when water is added to the snow surface. At this point the seasonal layering is not affected by the water, but the stability might be reduced if the water added comes as rain, and thus adds mass and stress to the snowpack structure. The next step is when the water has begun percolating further into the snowpack and might be wetting weak layers. As weaker layers often cause density transitions in the snowpack, water might pond here, if only for a while, and cause even weaker layer properties over the still dry snow. In the third and last step, the snowpack is drained, and preferential flow channels are formed. At this point the snowpack is expected to be isothermal and in a high-speed metamorphism towards a homogenous layering, which is positive for snow stability (McClung and Schaerer 2006, Tremper 2008).

2.5 Thermal behaviour/properties

Snow consisting of three phases, ice lattice, air and water vapor. The components of snow make the heat transport more complicated for snow, than for solid materials.
The heat in snow, either it is applied or subtracted, is transferred within the snow primarily by two mechanisms, conduction and vapor diffusion. Conduction happens through the network of ice grains and bonds and diffusion happens through the air-filled pore spaces (McClung and Schaerer 2006).

2.5.1 Thermal conductivity

The thermal conductivity is defined as the proportionality between the heat transport and the temperature gradient (Sturm, Holmgren et al. 1997).
The thermal conductivity for a solid, with unidirectional steady-state heat flow is defined by Fourier's equation:

$$Q = -k \cdot \frac{dT}{dz} \quad (1)$$

Where Q is the heat flux, k is the thermal conductivity and $\frac{dT}{dz}$ is the temperature gradient.
Because snow is a porous material, the processes that contribute to the temperature exchange within a cold snow cover is; conduction through ice rigid matrix, conduction through the air pores and latent heat transport through the pores due to sublimation and condensation of water vapor. Because of this complexity, the three mechanisms of heat transport are combined as the effective thermal conductivity and the Fourier's equation then becomes:

$$Q = -k_{eff} \cdot \frac{dT}{dz} \quad (2)$$

The conduction through the rigid ice matrix is about 100 times more effective than the air in the pore spaces (at 0° C: k_{ice}=2,24 W $m^{-1}K^{-1}$, and k_{air}=0,024 W $m^{-1}K^{-1}$).
It is difficult to apportioning the total heat transport into transport mechanisms since the temperature and water vapor gradient in snow are coupled and depending on the microstructure, which is difficult to quantify. Sturm, Holmgren et al. (1997) state that conduction trough air in the snowpack plays an insignificant role, and that vapor transfer of latent heat of condensation/sublimation in the pore space can increase the heat transferred along a temperature gradient by up to 50 %. The vapor transport and hence the latent heat

transfer that occurs as vapor is evaporated or sublimated from a warmer grain surface and either condensates or re-sublimates onto a relatively colder grain surface within the snowpack. It can also diffuse through the snowpack trough pore space. The effective thermal conductivity generally increases with snow temperature and therefore will the latent heat transfer increase as well.

There have been many studies that relates the snow density to the effective thermal conductivity, and Sturm, Holmgren et al. (1997) made an extensive review where they give a general relationship for k_{eff} (equation 3):

$$k_{eff} = 0{,}138 - 1{,}01\rho + 3{,}233\rho^2 \quad [0.156 \leq \rho \leq 0{,}6]$$
$$k_{eff} = 0{,}023 + 0{,}234\rho \quad [\rho < 1{,}156] \tag{3}$$

with values for ρ in g cm^{-3}. In the same study they collected all previous studies conducted about effective thermal conductivity of snow in one graph, showing the variations in the relationship between density and k_{eff} (figure 3). In 2011, Calonne, Flin et al. (2011) carried out numerical simulations of the conductivity of snow using microtomographic images. Their values were, as previous, strongly correlated to the density, and their explanation for the slight deviation to the regression curve to snow density were the effect of the anisotropy of k_{eff}. The snow thermal conductivity varies in the range 0,025-0,65 W m^{-1} K^{-1} (Sturm, Holmgren et al. 1997). The anisotropy plays an important role considering k_{eff}, as it behaves very different for different types of snow crystals. The vertical component of k_{eff} in facetted– and depth hoar crystals are up to 1,5 times larger than the horizontal, while for rounded grains the ratio is inversed. When measuring the thermal conductivity of snow, the accuracy is highly depending on the thermal anisotropy. The impact the microstructure of snow has on the anisotropy of k_{eff} builds up under the idea of snow as a monomineralic rock, one cannot consider the snowpack to consist of individual crystals in undisturbed form, but as a porous rock with bonds leading energy in different directions (Riche and Schneebeli 2013).

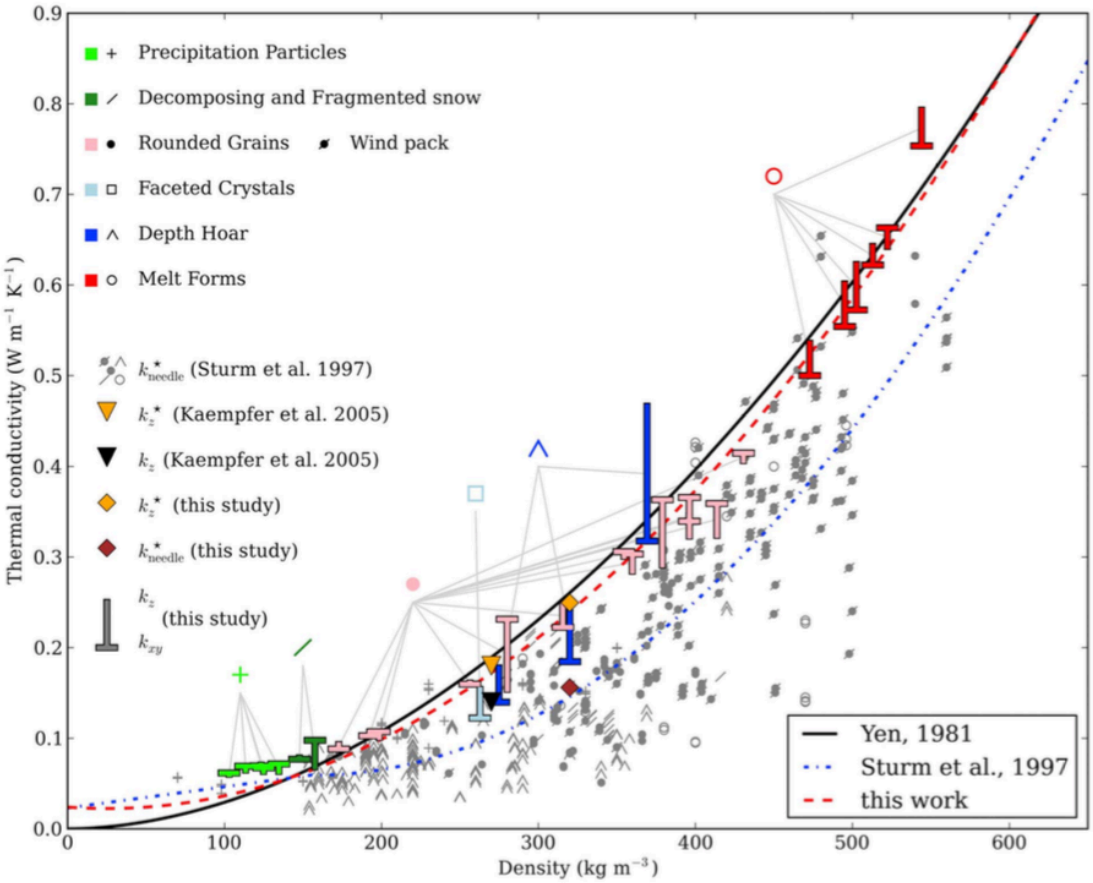

Figure 3: Graph showing the results of three different studies of the correlation between snow density and thermal conductivity of snow. The regression lines are from Yen (black solid), Sturm et al. (blue dashed) and Calonne et al. (red dashed). The T shape symbols represents the vertical component of k for the different grain types (Yen 1981, Sturm, Holmgren et al. 1997, Calonne, Flin et al. 2011, Domine, Bock et al. 2011).

2.5.2 Heat capacity

The heat capacity of a substance is the amount of energy required to raise its temperature by one degree, and the specific heat of snow is the amount of energy required to change the temperature of an amount of snow. Because snow consists of the three components ice, air and water vapor, the equation (4) to calculate the specific heat is then:

$$c_{p,s} = (\rho_a \theta_a c_{p,a} + \rho_i \theta_i c_{p,i} + \rho_l \theta_l c_{p,l})/\rho_s \quad (4)$$

Where $c_{p,s}$ is the specific heat of snow, $c_{p,a}$ is the specific heat of air, $c_{p,l}$ is the specific heat of water. The ρ and θ is the density and volumetric fraction of the respective components. At 0 °C and 1 atmosphere, the specific heat values are as follows; air = 1005 J kg^{-1} K^{-1}, ice = 2114 J kg^{-1} K^{-1}, water = 4217 J kg^{-1} K^{-1}. Based on equation 4, the specific heat of snow at 0 °C is 1977 J kg^{-1} K^{-1} with a snow density of 380 and zero water content. The variations in

specific heat based on which temperature it is measured, makes the specific heat of snow slightly temperature dependent (Armstrong and Brun 2008).

2.6 Near infrared photography

Near infrared photography maps the reflectivity of snow at around 870 nm wavelength and is a unique and effective method to objectively document the stratigraphy of a snowpack. The physics behind this technique is that ice is becoming about exponentially more absorbing in longer wavelengths, and coarser snow reflects less than fine grained snow (figure 4). In the near-infrared, coarse snow appears dark grey, and fine new snow appears almost as white as in the visible spectrum for humans. The images can be processed to derive the specific surface area of snow, an important property when considering the snow microstructure, or the images can be used to visually underpin the more traditional snow pit measurements (Matzl and Schneebeli 2006).

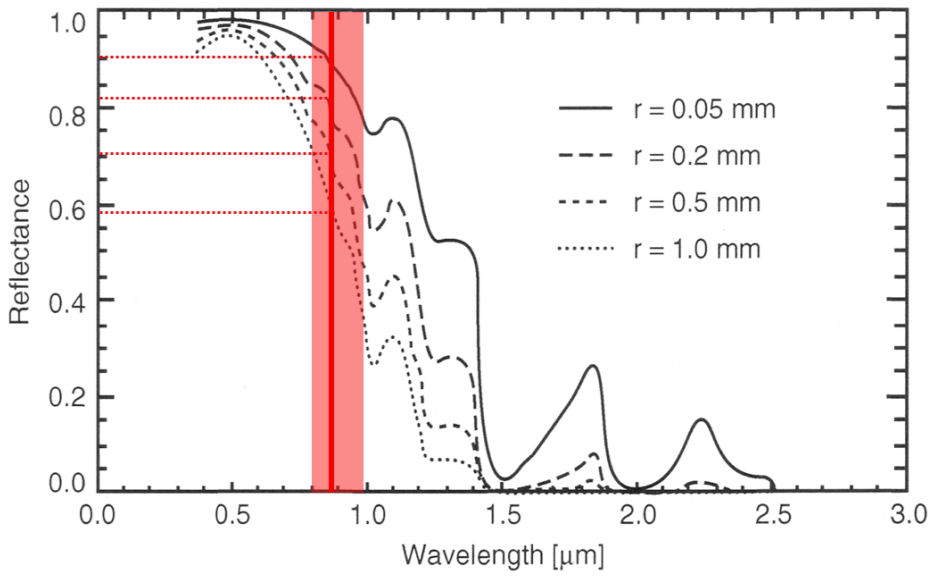

Figure 4: Graph showing the relationship between wavelengths and reflectance of different grain sizes (r). The smallest grain with r = 0,05 mm has the highest reflectance (Warren 1982).

3 Method

3.1 Field site

The study area is located at Finse, an alpine mountain area in the northern part of Hardangervidda. Finse train station (1222 m a.s.l.) is the highest point along the railway between Oslo and Bergen (east-west), as well as being the area for the weather divide between east and west (figure 5).

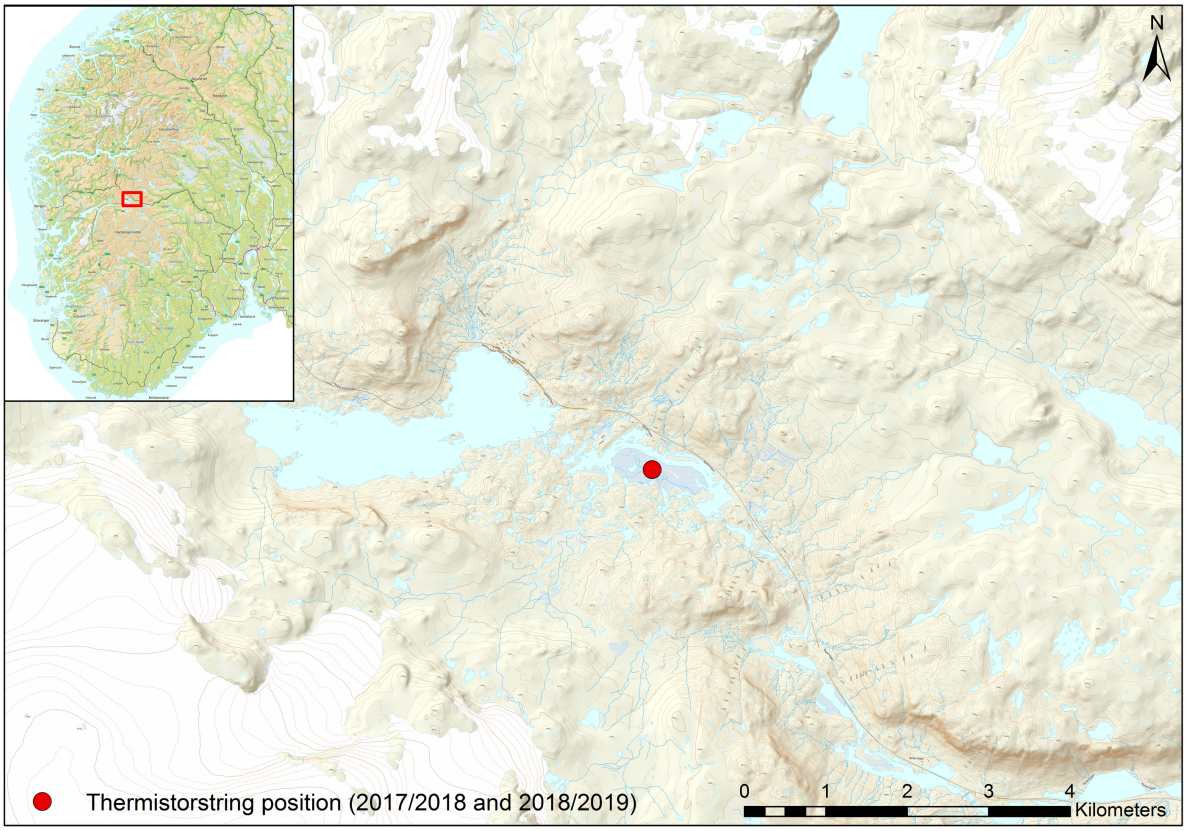

Figure 5: Map overview of the study area, Finse. The red dot marks the area where the thermistorstrings were deployed, about 2 kilometres east of the lake Finsevatnet. The glacier Hardangerjøkulen is situated in the bottom left corner of the map.

Finse becomes a natural site for field work projects because of the accessibility by train and the Finse Alpine Research Center, a station with everything needed for a practical and comfortable field campaign. The center belongs to the faculties of mathematics and natural sciences at the universities of Bergen and Oslo.

At Finse the two field winter seasons, the average air temperature -1,5 °C for 2017/2018 and 0,1 °C for 2018/2019. In terms of deviation to the normal period (1961-1990) was 0,8 ° and 2,4 ° respectively. The precipitation was 114 % and 94,9 % of the normal period (yr.no).

3.2 Field observations

The field work has been done in conjunction with field campaigns together with the research group LATICE (Land-ATmosphere Interactions in Cold Environments) at the Department of Geosciences at the University of Oslo.

3.2.1 Field work data

An important feature of the fieldwork was to dig snow pits. The pits were dug in the marsh at Finse, close to the temperature sensors and the mobile flux station, on relatively flat terrain. The pits were made about once each month, except for February.

The pits were dug during Finse field trips, with about one month's interval during the time the thermistor string were out. The recorded snow pits are from:

Table 1: Date and coordinates for snow pits.

Date	Coordinates (latitude/longitude)
05.03.2018	60.59024 / 7.53567
05.04.2018	60.58839 / 7.5293
04.05.2018	60.58997 / 7.53554
03.12.2018	60.59006 / 7.53562
21.01.2019	60.58972 / 7.535
26.02.2019	60.58967 / 7.53553

Objectives of snow pits

The objective of digging the snow pits was to get validation data for modelling. Because snow is as physically unstable as it is, having data showing the reality is of high value when considering model outputs.

3.2.2 Equipment

During field work at Finse, all transportation was done by skis, making standard skiing equipment a necessary part of the equipment list together with a snow study kit, shovel, avalanche probe as well as personal equipment for spending time outdoors for hours. Table 2 lists the used equipment.

Table 2: Equipment used for field

Snow study kit	Personal equipment
Shovel	Skis, ski boots, poles
Avalanche probe	Backpack
Folding ruler	Cell phone with GPS and map application
Field book and pencil	Food
Magnifier 25x	Thermos with warm drink
Crystal card	Extra clothing for standing still
Digital thermometer	Sunglasses/skiing goggles
Density cutter	
Brush	
Spatula	
Near infrared camera	
Frame holding reflectors for infrared camera	

3.2.3 Data logging in the field

After deciding the pit position and digging the pit, the metadata for the respective day and pit were recorded in the field book. Recorded data were time, date, coordinates, participants, altitude, exposition and meteorological data such as:

- Sky cover
- Precipitation type
- Air temperature
- Wind direction and strength

The air temperature was measured by placing the thermometer at a shadowed area well above the surface, i.e. behind a standing ski. Wind direction and speed was recorded based on experienced guessing. Figure 6 shows the snow pit of 26th of February, with sun hitting the back wall of the snow pit.

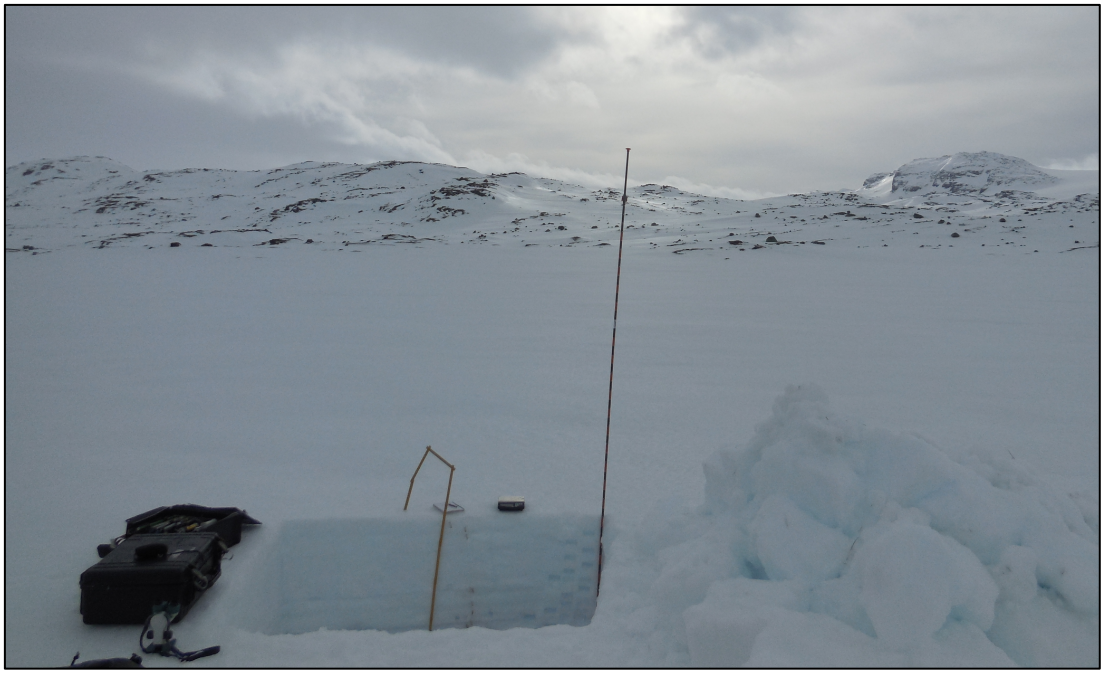

Figure 6: Picture of a snow pit dug the 26th of February 2019. Picture is taken towards south-west.

Snow pit procedure

The snow pits were dug at locations close to the thermistorstring without disturbing any other instrument in the marsh, and with a representative snow cover. At the marsh the terrain is fairly similar throughout, but to make sure the snow depth was even throughout the pit, simple depth measurements with avalanche probe was done. At the marsh there are some streams as well as the Finse river, and it was also made sure the pit wasn't dug over any of those, just by checking position on mobile phone apps such as "Norgeskart". An issue at Finse that occurres when digging pits on the flats, is to make sure to throw the snow in the direction approaching the pit, not towards the pit wall side. The direction of the pit walls was chosen either to prevent insolation from the sun on the snow, or to make the time spent in the pit the most comfortable in regard to wind and blowing snow. To prevent digging pits at the same locations, the coordinates for each pit was collected in a document.

The recording of the snow pit properties was conducted similar for all pits. Starting with measuring the total snow depth with a folding ruler and marking the obvious layers to get an overview of the entire snowpack. The detailed properties were recorded by starting from the top of the snowpack working down layer by layer recording grain type and size, hardness and moisture content based on the international classification of snow by Fierz, Armstrong et al. (2009). The classification of grain type and hardness are shown in respectively table 3 and table 4. The temperature was recorded simultaneously, with snow surface as first measurement and successively measured downward every 5 or 10 cm, depending on the snow depth.

Table 3: Snow grain form classes from Fierz, Armstrong et al. (2009)

Class	Symbol	Code
Precipitation particles	+	PP
(Machine made snow)	⊙	MM
Decomposing and Fragmented precipitation particles	/	DF
Rounded grains	•	RG
Faceted crystals	□	FC
Depth hoar	∧	DH
Surface hoar	∨	SH
Melt forms	o	MF
Ice formations	▬	IF

Table 4: Hardness of deposited snow from Fierz, Armstrong et al. (2009)

Symbol	Hand test	Term
F	Fist	Very soft
4F	Four fingers	Soft
1F	One finger	Medium
P	Pencil	High
K	Knife	Very hard
I	Ice	Ice

The density measurements were conducted by using a density cutter. The type of density cutter used was a box cutter with a volume of 100 cm^3. Measurements was taken such that there was no overlap between the samples, covering the whole snow pit depth. The weight of the samples was recorded with either a manual spring weight or a digital weighing plate, depending on the temperature as the digital scale has an LCD screen that is sensitive to cold temperatures. With the manual spring weight, the procedure was to put the sample in a small plastic bag attached to the weight. With the digital weight, the procedure was to weigh both the snow sample and the box cutter and subtracting the weight of the cutter later on.

3.2.4 Data logging after field

The field notes were as part of post processing registered into a snow profile visualisation tool from www.niviz.org. The snow pits registered in Niviz can be exported as either caaml6 or jpeg file format.

3.2.5 Near infrared photography

The near infrared images were taken with a normal digital camera where the near-infrared blocking filter has been removed and replaced with a NIR-transmitting filter. The images were taken after finishing the traditional snow pit measurements, and cleaning the pit wall, providing it to be as flat as possible with available gear. Normally the cleaning was done by using the shovel first, second a spatula for more control, especially on ice layers, and lastly a brush with horizontal strokes to "freshen" the surface. The images must be taken in diffuse light, so if the sky was clear and there was sun, a small shadow tent (typically used at the beach to shelter i.e. kids) were used to provide shadow. To be able to trace the position of the images on the pit wall, either a folding ruler or an avalanche probe with metering points were set up along the pit within the image frame.
The post processing was to edit the images into black and white, fix contrast, exposure, brightness, levels and curves in image processing software.

3.3 Instrument

In order to measure snow temperature a thermistorstring were built. Due to a shutdown of the instrument in the end of winter 2017/2018, a new one was built for winter 2018/2019. The strings consisted of respectively 20 and 40 sensors every ~10 and 5 cm. The distance between the sensors on the 18/19 version were shortened to provide a better resolution.

3.3.1 Sensor

The sensors used are the DS18B20 from Maxim Integrated Products. They provide 9-bit to 12-bit Celsius temperature measurements and communicates over a one-line bus that by definition requires only one data line together with ground for communication with a microprocessor. The sensors have a 64-bit serial code, which allows multiple sensors to function on the same 1-wire bus. The manufacturer gives an accuracy of ±0,5 °C from -10 °C to +85 °C (MaximIntegrated 2018).

3.3.2 Sensor testing

To make sure the sensors performed within the manufacturers promise of accuracy, the sensors were tested in a cold chamber at the University before assembling the string. The cold chamber is a CTS Pro 4.02 (ControlTecnica 2018) and allows the user to control the temperature. In order to test sensors in a representative manner, a program with temperatures going from air temperature to -20 °C, back to +20 °C with a stop for 10 minutes every 5 °C was used. This reference data made it possible to remove sensors with accuracy of more than ±0,5 °C. Figure 7 shows the setup for testing the sensors in the cold chamber. The DS18B20 sensors are at this point still fixed to the boards from the manufacturer. The sensors were connected on the boards in a way that made it possible to connect the boards as well, and thus test more sensors on the same 1-wire bus.

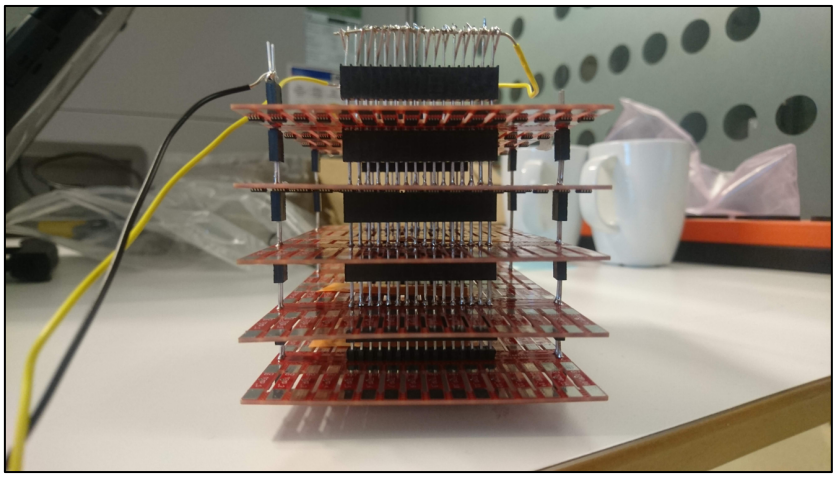

Figure 7: The set-up of the sensors for testing in cold-chamber. Each sensor is connected on the same 1-wire bus making it possible to read all sensors at the same time.

3.3.3 Building Hardware

When assembling the thermistorstring, the sensors were organized in respect to serial number, since the microprocessor reads the sensors in that order. The sensors were then soldered to pre-cut pieces of cable, and each sensor got covered in heat shrinking tube with glue to provide them to be waterproof.

2017/2018

The first field season, the assembly of the thermistorstring was relatively simple consisting of a 50 mm diameter PVC pipe with the wire with sensors taped outside with transparent duct tape. Due to a weakness in the code reading the data in the microprocessor, the first edition consisted of two strings of 10 sensors each. This because the code had a restriction in amount

of data it would read. Thus, the strings were taped on in series from the lower end and up. To prevent an extra cable running along the top sensor string, a hole was drilled in the pipe where the lower string ended. The strings were merged at the top of the pipe, and the cable to the box with the microprocessor were laid out with enough slack to account for the tension arising from the coming snow. The metal post holding the box with the microprocessor were standing about 3 meters away from the thermistorstring.

2018/2019

For the second field season, it was decided to increase the frequency of sensors, and to implement that, two strings with 10 cm distance was built. The idea was to mount them on the PVC pipe with a 5 cm shift between the strings. The setup of the pipe was also slightly different the second year, as this year the distance to the metal post holding the microprocessor was only about 1 meter. The short distance allowed to use it as support for the PVC pipe. Therefore, a t-joint holding a horizonal arm (also PVC) reaching from the vertical pipe to the metal pole was mounted. The arm was connected to the metal post with a pipe clamp. The pipe with the sensors attached got covered in heat shrinking tube to make it waterproof. An advantage of using PVC pipes is that it allowed to hold the cables inside the pipes and then pull them up along the metal post to the microprocessor. This prevented any loose cables hanging in the air/snow between the microprocessor and the thermistorstring pipe. Figure 8 show the thermistorstrings taped to the pipe before deployment.

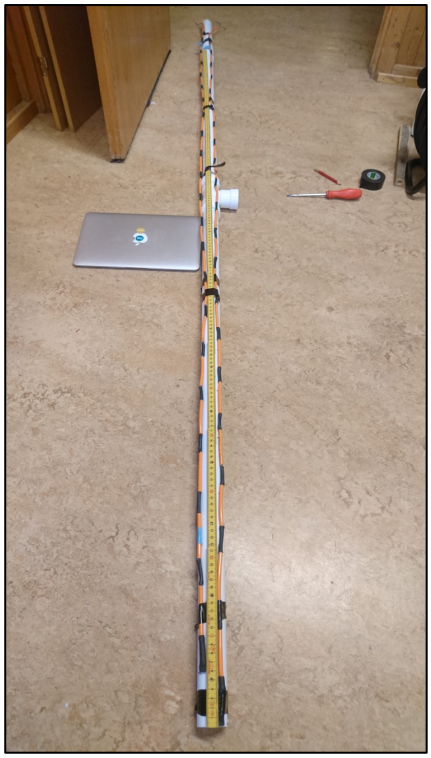

Figure 8: The 2018/2019 edition during assembly inside the research station at Finse. Picture taken after taping string to the pipe and before covering the pipe with heat shrinking tube.

Power supply

The power issue was solved by setting up a solar panel of 3,5 W and a battery with capacity of 6600 mAh. And with an energy consumption from the microprocessor of 17 mA while on and 30 µA during sleep, the energy capacity was adequate. During both winters the battery level were kept stable between ~92-100 % (figure 9).

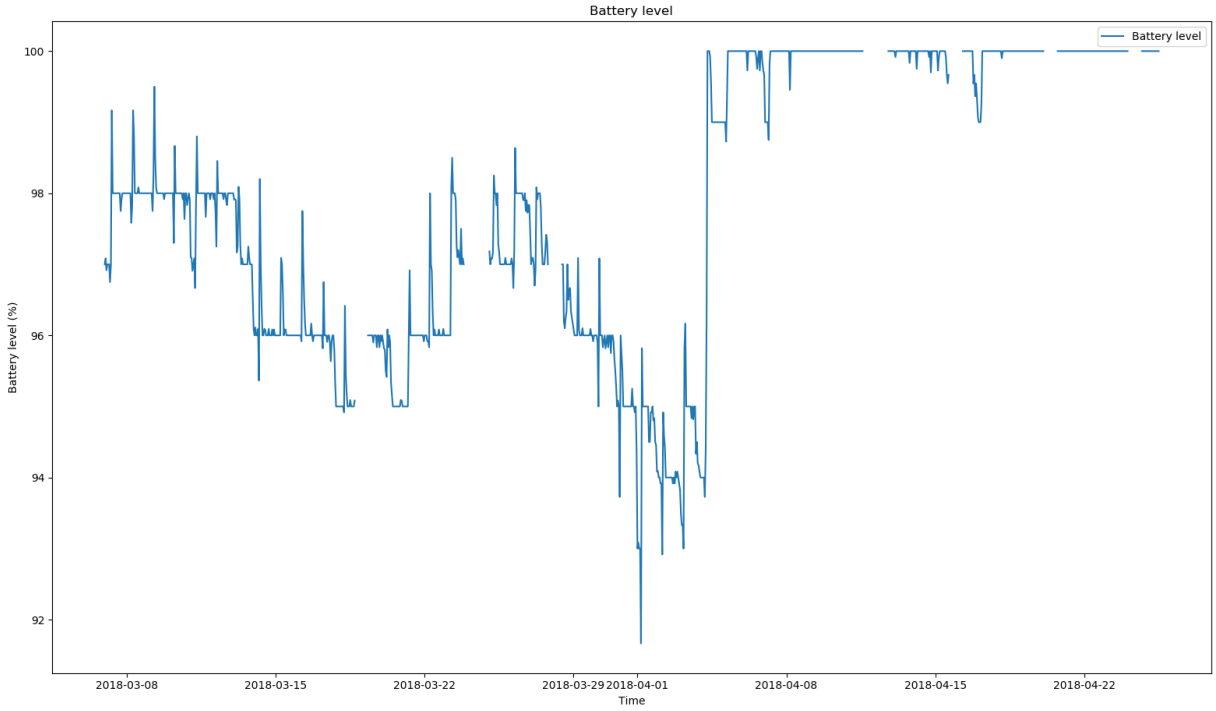

Figure 9: Battery level during the first field season. The small gaps in data is due to data transmission issues.

3.3.4 Deployment

The deployment of the thermistorstring were conducted slightly different for the two winters due to the concept of learning by doing as well as better time for planning before the second season. Figure 10 shows pictures of the two setups in field.

2017/2018:

The first edition was deployed 06.03.2018, and at this time the snow depth was about 160 cm. Because of the snow depth and several ice-layers within the snow, a regular avalanche probe was used to create a path for the pole. The lowest 12,5 centimetres were too hard to penetrate and hence became the position of the lowest sensor that winter.

2018/2019:

The second edition was deployed 04.12.2018. Earlier that fall ground anchors had been installed to be base for the metal post supporting the thermistorstring. The snow depth at the time was only 34 cm, and it was considered convenient to dig to the ground at the position of the thermistorstring to have it to start from zero. Already the next morning the area was filled up with new snow.

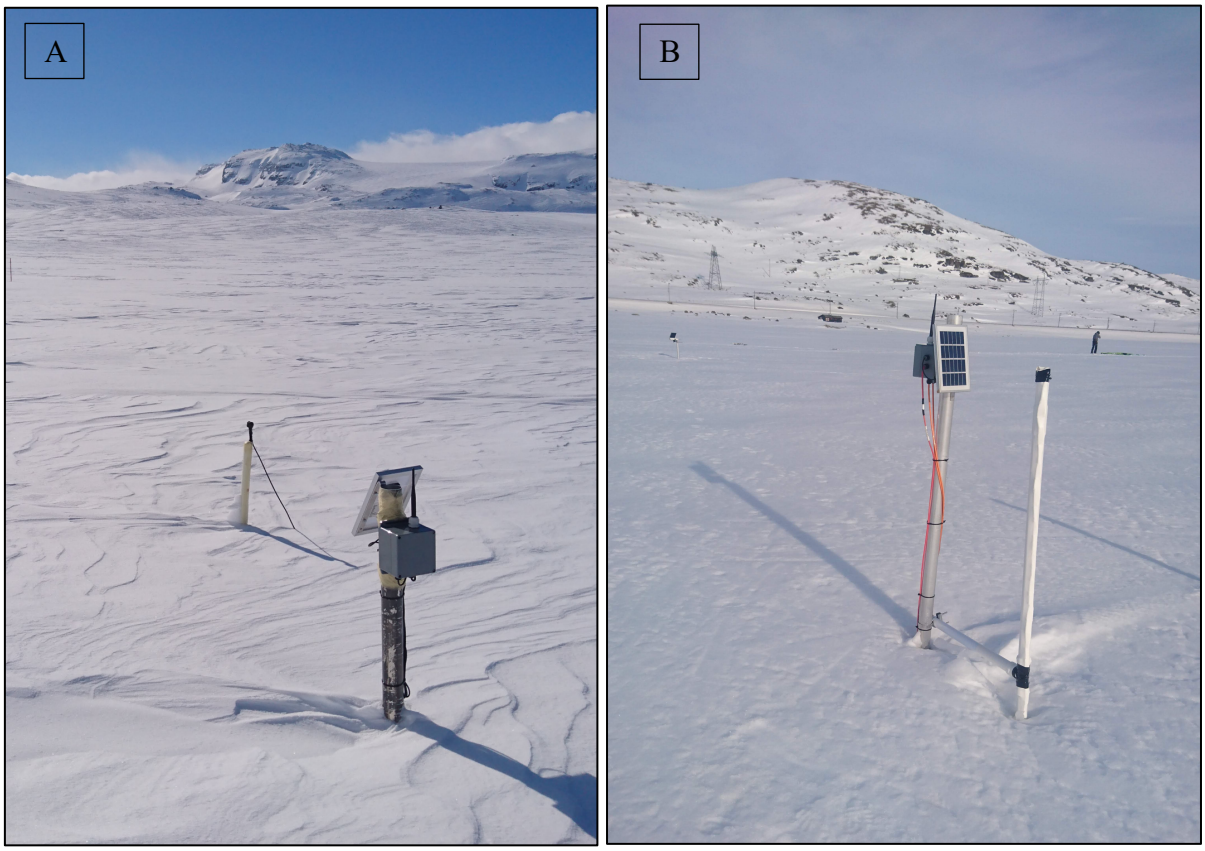

Figure 10: The instrument set-up for the winter 2017/2018 (A). The thermistorstring in front and the metal post with the solar panel and the box with battery and microprosessor. Picture B, is of the set-up for the second edition (2018/2019), here with the supporting arm barely over the snow surface.

3.3.5 Retrieving data

The microprocessor that was used is a Waspmote from the tech company Libelium. The Waspmote reads data and sends it through radio signal. At Finse the Geoscience department at University of Oslo has developed a wireless sensor network consisting of a number of Waspmotes in connection with different instruments, and each Waspmote has a function as a router in the network. This creates a mesh network, which means that if a neighbouring Waspmote stops working, the distance to the next will be so short that the data will reach the

end station regardless. The end station in this case is inside the Finse Research station where the data is sent to servers by internet. Figure 11 shows the inside of the box holding the Waspmote and the battery (S.L. 2019).

Figure 11: Picture showing the inside of the box holding the Waspmote and the battery.

3.4 External validation data

The University of Oslo had stationed a mobile flux station at the marsh from January 2018 to March 2019. The flux station is a fully operating energy flux measurement tower with equipment covering eddy covariance, ground heat flux, radiation, snow depth, air temperature, surface temperature, precipitation and wind speed and direction.
As validation for my work the snow depth and air temperature were retrieved to support the modelling and processing of data.

The snow depth is measured by an ultrasonic sensor that measures the distance to the snow surface from a fixed position. The snow depth is derived by subtracting the distance to the snow surface from the height above the ground surface which the sensor is mounted. The height of the sensor was 300 cm.
The air temperature at the mobile flux station is measured in a radiation shield.

3.5 Modelling

The principle of the water content estimation is to simulate the temperature evolution with a model that is written for a dry snowpack, hence it does not account for refreezing. By calculating the refreezing capacity of both the measured and the simulated temperature and then consider the deviation between those, the water content can be derived.

3.5.1 The model

The data the model uses to do simulations is the measured snow temperature and air temperature. Because the snow depth is dynamically changing during the winter, the measured snow depth is used to limit the simulation to the actual snow depth.
The model uses the first temperature profile from the measured snow temperature as basis for further simulations. For the rest of the simulation, the model uses the air temperature together with input parameters for snow properties. The input parameters are density, thermal conductivity and heat capacity, and the values that was used are shown in table 6.
The quality of the simulated result was tested against the measured by subtracting the simulated values from the measured and plotting the result.

Table 7: Input parameters in the model, k, ρ, C.

Variable	Values
Thermal conductivity - k	0,15 (W m^{-1} K^{-1})
Density - ρ	390 (kg m^{-3})
Heat capacity - C	800 (J kg^{-1} K^{-1})

3.5.2 Estimation of water content

With an adequate simulation result in terms of expectation, the refreezing capacity of both the simulated and the measured temperature were calculated by using the equation 5 (Marchenko, van Pelt et al. 2018) below:

$$RC^{sim} = T^{sim}\rho C\Delta z$$
$$RC^{meas} = T^{meas}\rho C\Delta z \quad (5)$$

Where $RC^{sim}$and RC^{meas} is the refreezing capacities of the simulated and measured temperatures respectively, T^{sim} and T^{meas} are the simulated and measured temperatures, ρ

and C are the snow density and heat capacity used in the model, and Δz is the vertical grid step between the sensors.

Because the simulated temperatures not account for refreezing in the snowpack, it is expected that the difference between measured and simulated temperatures are due to refreezing and release of latent heat. The energy difference is converted into a quantity of water by using the equation 6 (Marchenko, van Pelt et al. 2018) below:

$$m_w = \max\left(0, \frac{RC^{sim} - RC^{meas}}{L}\right) \quad (6)$$

Where m_w is mass of water and L latent heat of fusion of water. $RC^{sim} - RC^{meas}$ gives a difference in energy per square meter (J m^{-2}) and by dividing with $L = 334000$ (J kg^{-1}) the result is kg per square meter (kg m^{-2}).

4 Results

4.1 Field work

4.1.1 Snow pit data

During the two winter seasons a total of six snow profiles were recorded in the marsh. All of the profiles included stratigraphy with grain type and grain size, temperature and density. In addition, three of the pits included near infrared images. The six snow profiles are shown in the appendix.

Stratigraphy

The snowpack during 2017/2018 were during the cold period evenly distributed between rounded grains (RG) and faceted crystals (FC), and the snow pit dug 4th of May consisted of melt forms (MF) with a few thin ice layers (IF). The yearly grain type distribution was then 30,2 %, 33,6 % and 24,5 % between RG, FC and MF respectively.

The winter of 2018/2019 the three snow pits recordings were of a different character. The pit from December 3rd was only 34 cm deep and consisted of either depth hoar (DH) or precipitation particles (PP) and defragmented particles (DF) with an ice layer dividing the DH from the rest. The 20th of January the snowpack consisted of mostly FC particles, a top section with RG, two layers of MF and nine ice layers. In the end of February, the snowpack was dominated by MF with five of the previously recorded ice layers in between, and the bottom few centimetres with DH. The yearly grain type distribution was then dominated by MF with 44,6 %, FC with 19,9 and RG with 10,3 %.

Table 8 gives an overview of the complete distribution for the two winter seasons.

Table 8: List of grain type in percentage

Grain type	2017/2018 (%)	2018/2019 (%)
RG	30,2	10,3
DF	2,9	5,0
PP	1,6	4,8
FC	33,6	19,9
DH	0	6,4
MF	24,5	44,6
IF	7,2	8,0

Density

The density values were measured for the whole snow depth and in table 9 the average values are listed for both winters.

The average density for the snowpack during 2017/2018 varied between 329 kg m^{-3} in the beginning of March up to 549 kg m^{-3} in the beginning of May, giving a seasonal average of 410,8 kg m^{-3}. The average values for the snowpack of 2018/2019 were a bit lower varying between 296 kg m^{-3} in early December to 441 kg m^{-3} in the end of February, giving a seasonal average of 373,3 kg m^{-3}.

Table 9: List density values, maybe only bulk

2017/2018	**Average density (kg m^{-3})**
05.03.2018	329
05.04.2018	358
04.05.2018	549
Seasonal average	*410,8*
2018/2019	-
03.12.2018	296
21.01.2019	383
26.02.2019	441
Seasonal average	*373,3*

Near infrared photography

The near infrared photograph (NIR) images have been used to visualise and trace layers in the snowpack. Figure 12, 13 and 14 show snow pit profiles with associated NIR images. The red arrows in the images marks the distinct properties and positions them in both the images and the profiles.

From the snow pit from 5th of March 2018 (figure 12), most of the sharp transitions are traceable. Such as the uppermost arrow marking the layer with mostly FC between two layers of RG. The ice layers are also possible to trace.

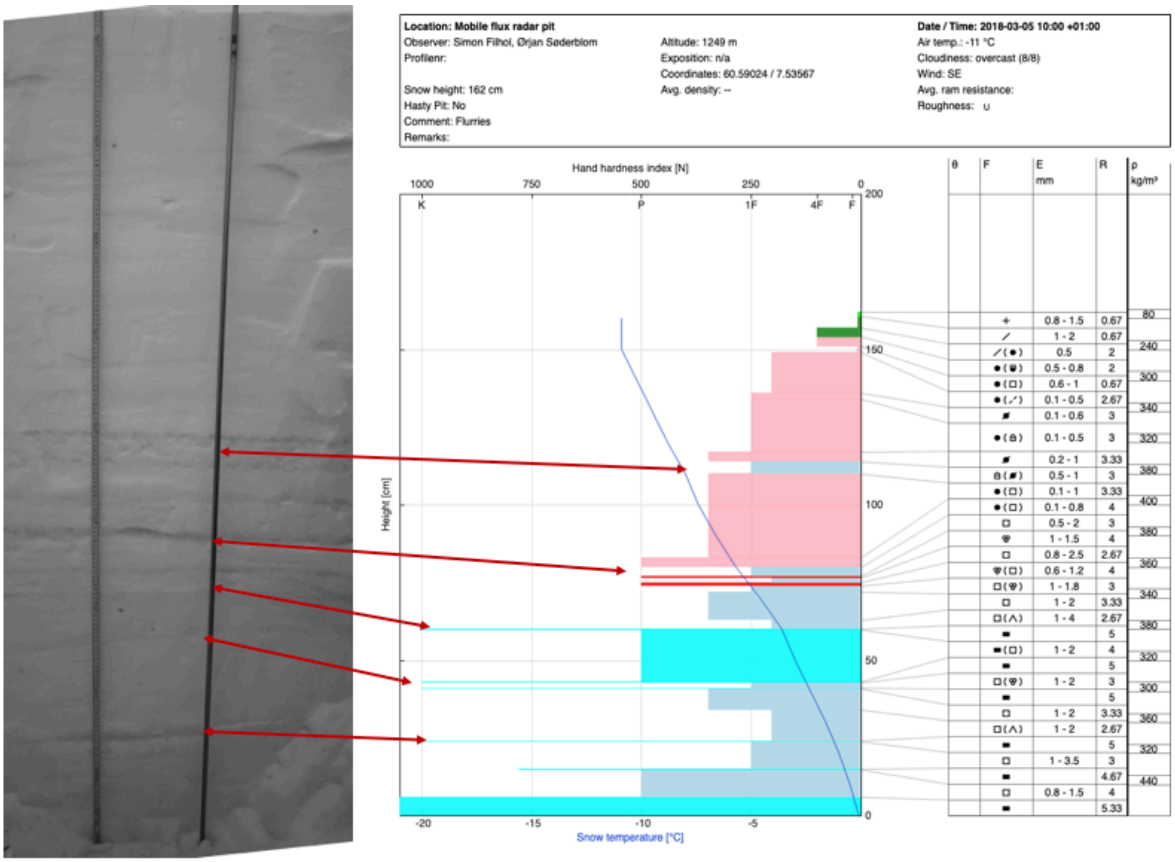

Figure 12: Comparison of near infrared image and the recorded snowpack properties the 5th of March 2018. The arrows mark the clearest correlations.

The snow pit from 5th of April 2018 (figure 13) was 215 cm deep, making it hard to cover the whole pit wall in one image, hence the composition of several images. In this pit, the transitions between RG and FC are traceable, as well as the ice layers such those pointed out with the second lowest arrow in the figure. The arrow points at the three ice layers just below 100 cm in the profile.

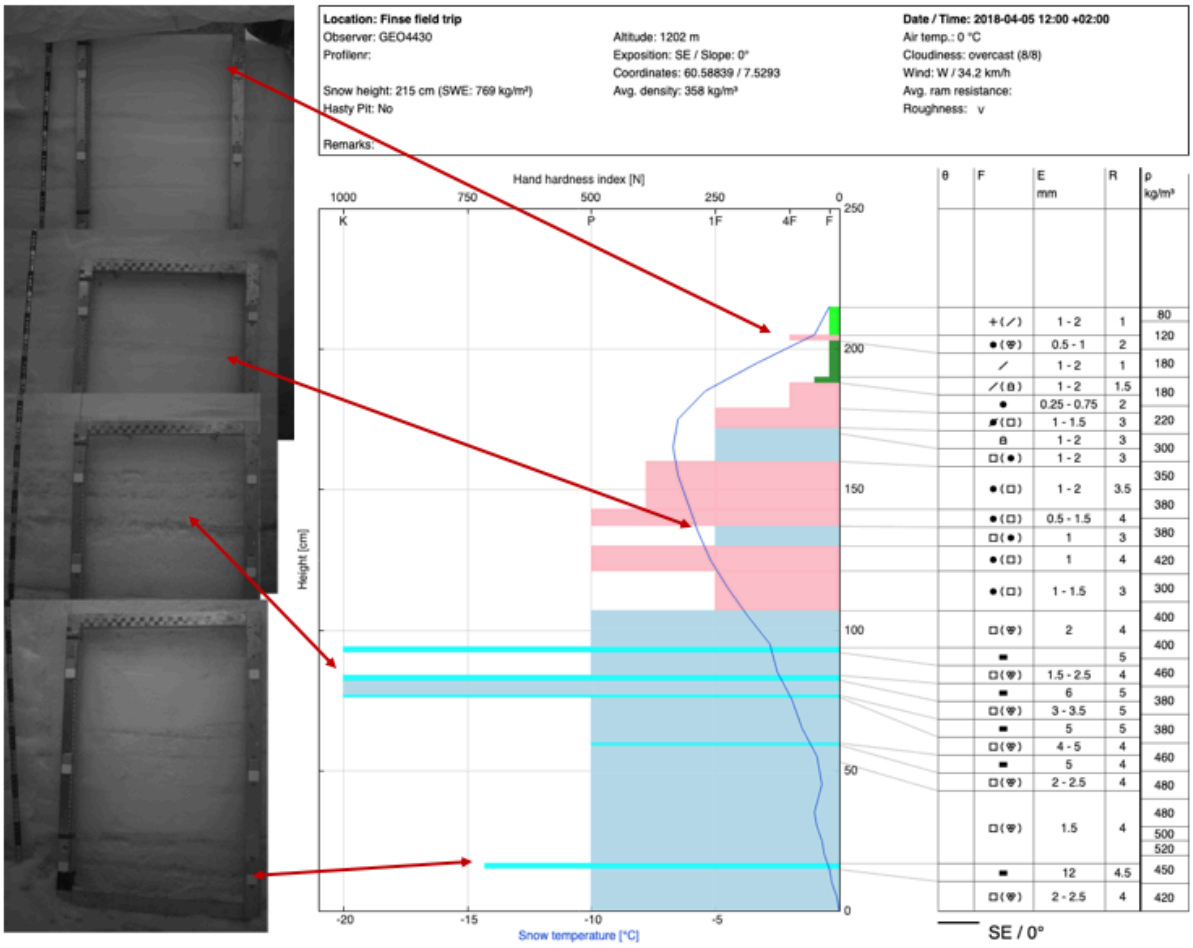

Figure 13: Comparison of near infrared image and the recorded snowpack properties the 5th of April 2018. The arrows mark the clearest correlations.

The snow pit from 12th of December 2018 (figure 14) was consisting of five layers, and with an ice layer being one of them causing there to be only two clear transitions, as the ice layer at the bottom is not visible in the image. Both of these are clearly traceable in the image. The uppermost is between a layer of PP and DF, with hardness of respectively fist and 4 finger/1 finger. The second feature in the image is the ice layer between the layer of DF and a layer of DH.

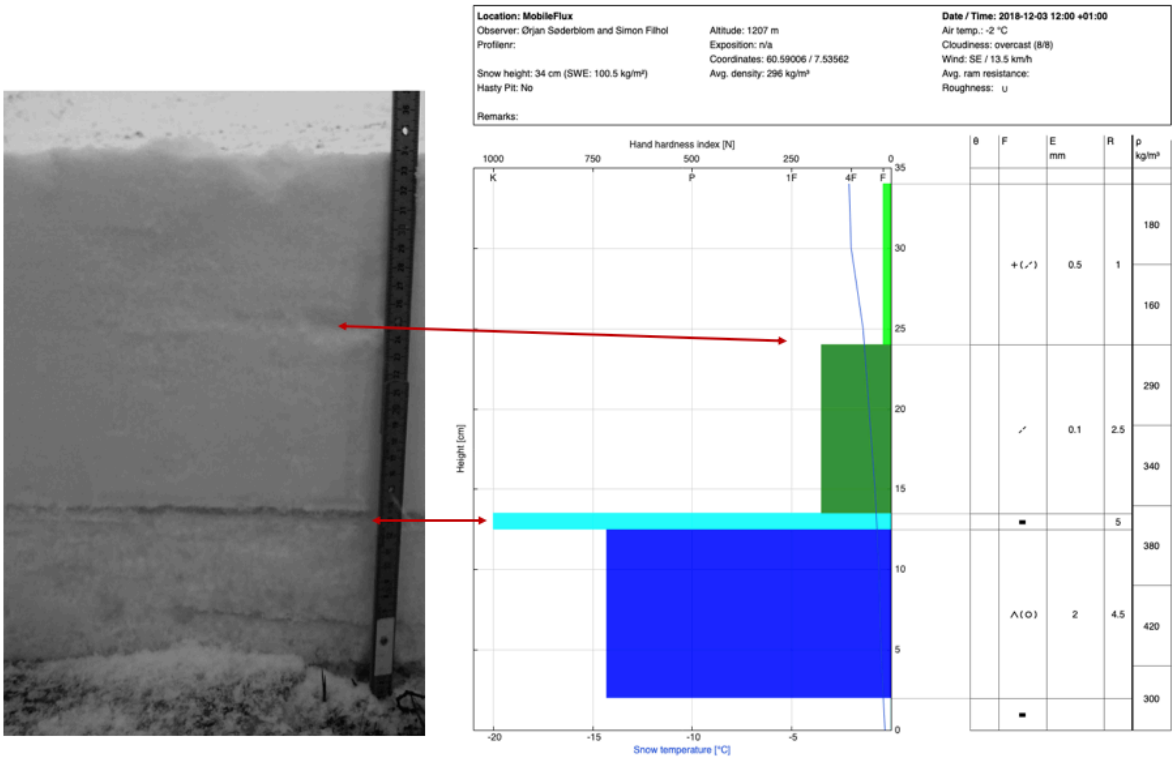

Figure 14: Comparison of near infrared image and the recorded snowpack properties the 12th of December 2018. The arrows mark the clearest correlations.

4.2 Instrument performance

The two thermistorstring editions was functioning for each of their winter seasons.

4.2.1 2017/2018

The first edition had no issues other than those before deploying until it broke down mid-April due to what seemed to be a shorting. It sent data the whole period from deployed to it broke down, a total of seven weeks covering both cold temperatures down to -30 and the period up to an isothermal snowpack. In figure 15, the temperature profile of both the snow pit and the thermistorstring the 5th of April 2018 are plotted for comparison. The difficulty of the plot is the difference in snow depth at the two positions, but there is a similar trend in the temperature profiles. The difference in snow depth between the two positions was 35 cm, and this is roughly the same distance as the shift in the temperature profiles. The thermistorstring measurement (blue line) is measuring 1,3 °C colder temperature where the profiles are at their minimum temperatures. The abrupt change in temperature in the snow pit measurement at about 50 cm is most likely due to measurement errors.

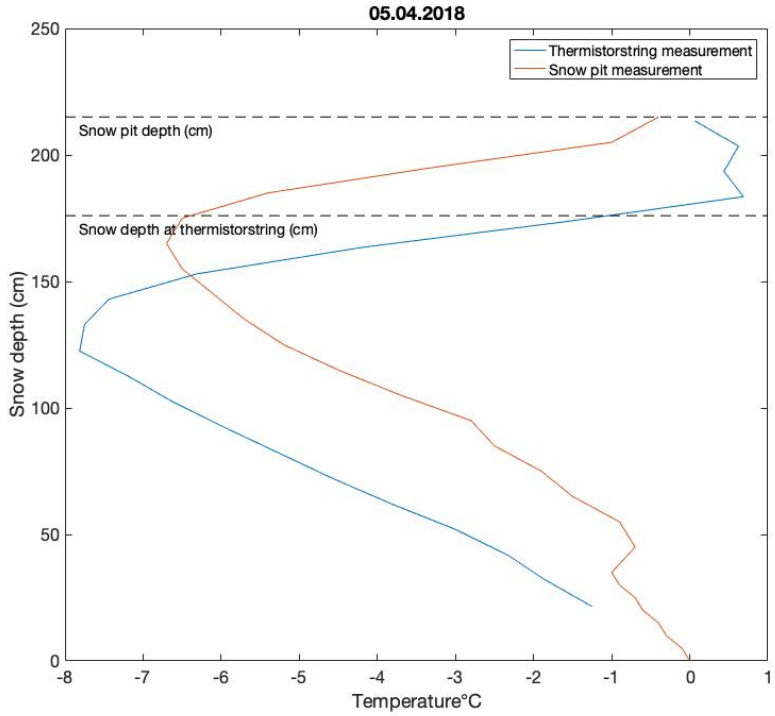

Figure 15: A comparison of the temperature profile measured in the snow pit and the thermistorstring the 5th of April 2018.

4.2.2 2018/2019

There was a shift in the temperature profiles also in the second edition (figure 16), but not as prominent as for the first. Due to a longer shutdown in 2019, the 20th of January is the only time with both a snow pit measurement and the thermistorstring operative. At that time the snow depth sensor at the mobile flux station was down, so the snow depth there cannot be used as reference in the figure. Based on the shift and the correlation between difference in snow depth and shift in the profiles, it can assumed that the difference in snow depth the 20th was approximately 5 cm. Different from the first edition, the thermistorstring measured higher temperatures than the snow pit, and opposite to the previous year the snow pit temperature profile measured just over 1°C lower temperature at the coldest position in the profiles.

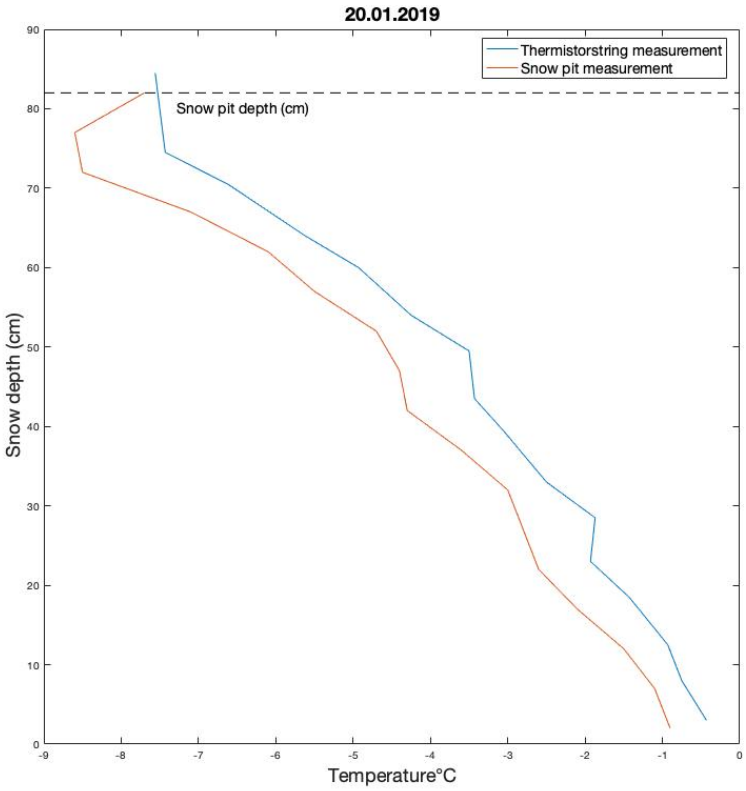

Figure 16: A comparison of the temperature profile measured in the snow pit and the thermistorstring the 20th of January 2018.

4.3 Temperature simulation

4.3.1 2017/2018

The observed temperatures are below 0 °C from the beginning of the dataset until the 8th of April when the top 0,5 meters starts to warm (figure 17A). The 14th of April there is a warming of the whole snowpack. The simulation (figure 17B) has a longer response period to warming which can be seen both in the first and the second cold front from the top of the snowpack (at about 18th of March and between the 30th of March to the 5th of April). The simulation needs more time to adjust to the air temperature.

Figure 17C shows the difference between the observed and simulated temperature. The simulated is subtracted from the observed, and therefore will positive values in the plot indicate warmer observed temperatures. Below -0,5 meters are the difference close to 0 with maximum difference of 2 °C during the period with a cold snowpack.

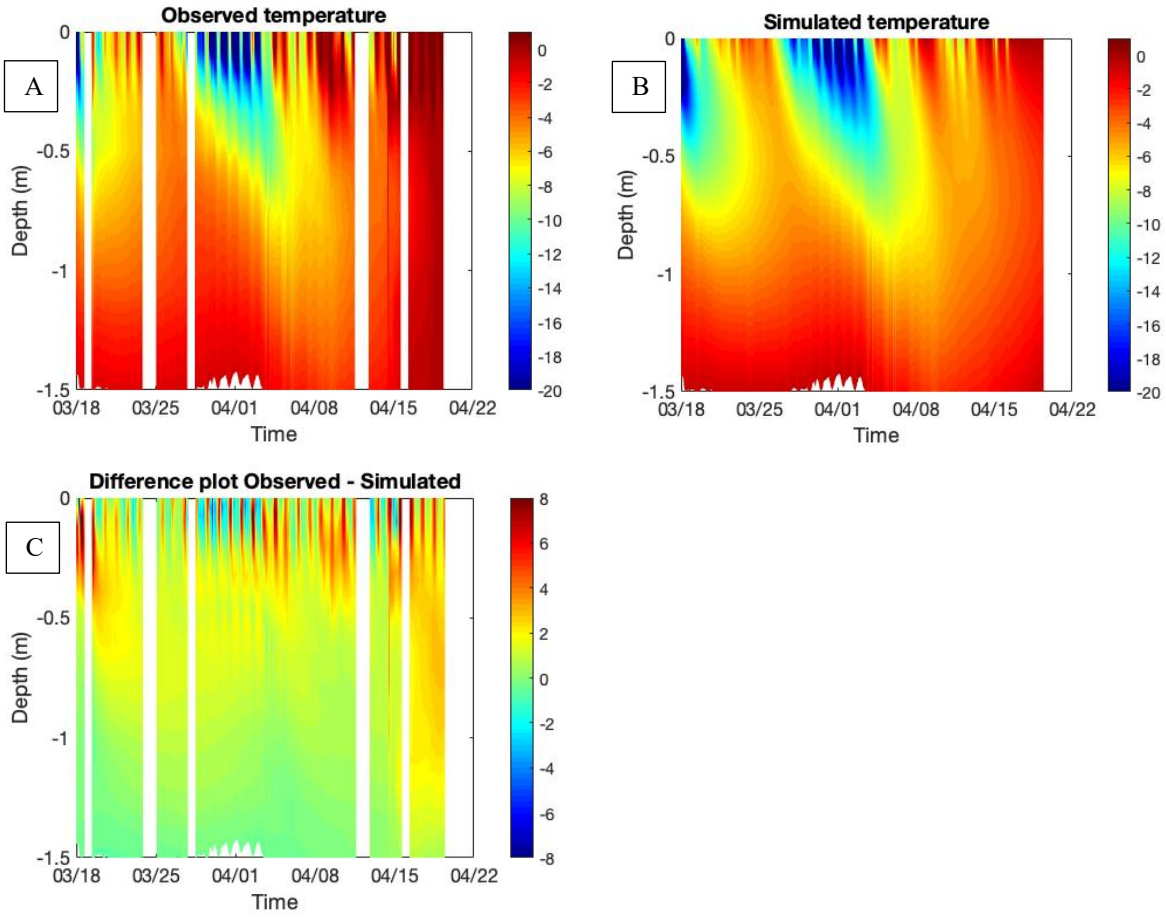

Figure 17: The three model output figures. A, is the observed temperature, B is the simulated and C is the difference between A and B.

4.3.2 2018/2019

The simulation of the 2018/2019 dataset were not conducted due to an error in the code in the microprocessor. The coding error caused problems with the process of saving and sending the data into the wireless network from start, and those stuck to the measurements for the whole winter. The reason for the mistake was a communication miss within the LatIce group and a coding update. Due to the error the processing of the data had to start with extracting the data from the log file, where all the information is listed as a text document, and the issue appeared when aligning the temperature data with other input data in the model.

4.4 Water estimation

4.4.1 2017/2018

The water content estimation for the first season show abnormally high water content (m_w) in the period with expectations of a dry snowpack. From the beginning of the time period to the 14th of April the m_w should ideally be 0, but instead the model estimates water contents of up to 0,9 kg m^{-2} with some fluctuations (figure 18). The increase in m_w the 14th of April corresponds to the increase in air temperature and observed warming of the snowpack. The water content increased to 2,25 kg m^{-2} at the end of the dataset, with a difference to the value before the expected increase of 1,72 kg m^{-2}.

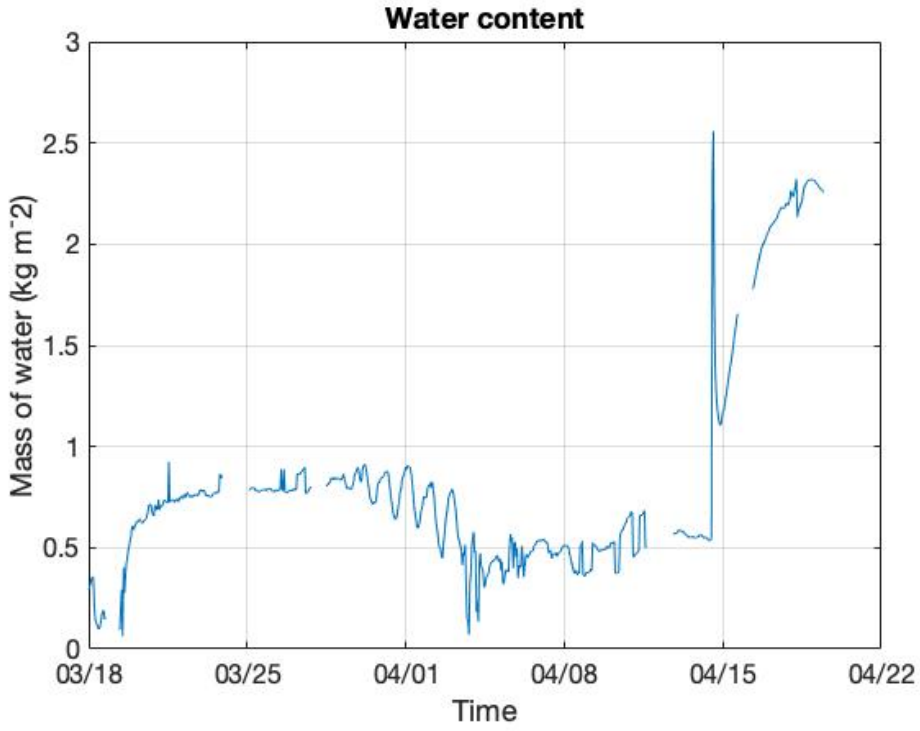

Figure 18: The result of the water content calculation. It is notable that the values up to the 14th of April is higher than zero. The maximum value in the melting period of the dataset is 2,3 kg m^{-2}).

5 Discussion

5.1 Field work

Field work in snow science is challenging in the way that it is highly subjective. The traditional way of recording snow properties, as done in this work, is depending on the abilities to the person doing measurements. Some of the measurement techniques is more relying on tool precision, such as the thermometer and the weight scale, but the remaining measurements conducted in this study is of a more train-and-learn character. All field work has been done by the author to provide a consistent implementation of the measurements. The field work has been conducted with the care and precision that can be obtained while taking human errors into account.

5.2 Instrument

5.2.1 Sensor accuracy

The temperature sensors were tested in the cold chamber, and the sensors that performed outside the expected accuracy as promised by the manufacturer of ±0,5° C got discarded. To improve the testing additional the assembled thermistorstrings could have been tested in the cold chamber to make sure no changes in the accuracy occurred during assembly. The thermistorstring could also been calibrated by having them in an ice bath, and further add or subtract the difference to the later measurements.

5.2.2 Robustness

Uncertainties following having a measurement tool within the snowpack during a whole season for non-invasive data collection are i.e. the interaction between the instrument and the snow, and the robustness of the instrument itself.

Regarding the interaction between the instrument and snow, a possible uncertainty source can be water following the pipe causing local heating of the snow around the pipe. If that happens, it can also be assumed to be created cavities around the pipe. Such cavities can further create local strong temperature gradients and hence a different metamorphism around the thermistorstring. The latter uncertainties questions whether an instrument like the thermistorstring performs unchanged during a whole winter season.

The measurements are also favourable of having a robust system, both in terms of hardware and software. The 2017/2018 edition broke down around the 20th of April most likely due to a shorting, but other than that is seemed to be good. The 2018/2019 edition was working in terms of hardware to the end of the winter season, but the software and coding was too weak.

5.3 Model

5.3.1 Choice of input parameters

As density of snow is a dynamic property because of metamorphic processes it varies a lot during a season. For winter 2017/2018, the average density increased from 329 kg m^{-3} in the beginning of March up to 549 kg m^{-3} in the beginning of May. This gives a difference of 220 kg m^{-3} over a period of two months. When considering the work of Calonne, Flin et al. (2011) the effective conductivity for the two densities would be 0,25 and 0,7 W m^{-1} K^{-1}. The end of the measuring period for that winter was the 20th of April and it is assumed that the density did not increase up to 549 kg m^{-3}, but due to a warming of the snowpack at that time it was probably higher than the measurement from 5th of April of 358 kg m^{-2}. The value used in the temperature simulation model was 380 kg m^{-2}, which is higher than the density of the cold snow period. As the work of Calonne, Flin et al. (2011) show, the density has a great impact on the effective thermal conductivity and choosing one value throughout the whole simulation period may cause difficulties when simulating. Both because the densities will vary in depth, but also in time.

Another factor controlling the effective thermal conductivity is the thermal anisotropy of snow. With a 1,5 times larger vertical component of k_{eff} for FC/DH than RG the distribution of snow grain type within the snowpack is of importance. For winter 2017/2018 the distribution throughout the season was as shown in table 8, 33,6 % and 30,2 % for FC and RG. It is therefore assumable that there is a possible deviation to the chosen value along the regression curve of 50 %.

5.3.2 Forcing data uncertainties

Air temperature

The measured temperature by the top sensor on the thermistorstring and the air temperature measured at the mobile flux station follows about the same phases, but the thermistorstring always measures higher temperatures at the phase peaks. This is expected to be due to the heating effect of radiation. Figure 19 show the two measurements over time. With differences of about 10° C at maximum, this causes obvious mismatch in the comparison of the outputs (figure 17).

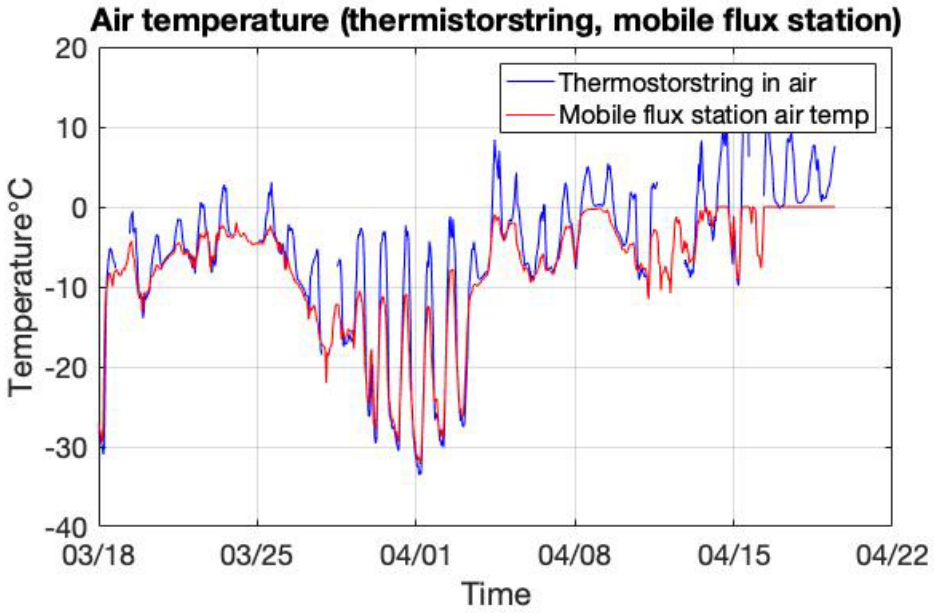

Figure 19: The air temperature evolution of winter 2017/2018 measured by the top sensor of the thermistorstring (blue line) and the mobile flux station (red line).

Snow depth

The model was forced with the measured snow depth at the mobile flux station which was situated a few meters away from the thermistorstring in 2017/2018. Figure 15 in chapter 4.2.1 show the difference in snow depth measured by the ultrasonic sensor and snow pits. It can be expected that this also accounts for the relationship between the thermistorstring and the ultrasonic sensor. The temperature model is sensitive to change in snow depth, and when considering the correlation between the spikes in snow depth and the strong differences in simulated and observed temperature in the top 0,5 m of the snowpack (figure 20), the snow depth can be assumed to be a possible cause. A positive temperature difference implies a warmer observation than simulation. The large offset in between the observed and simulated temperature made it meaningful to disregard the top 0,4 m in the simulation.

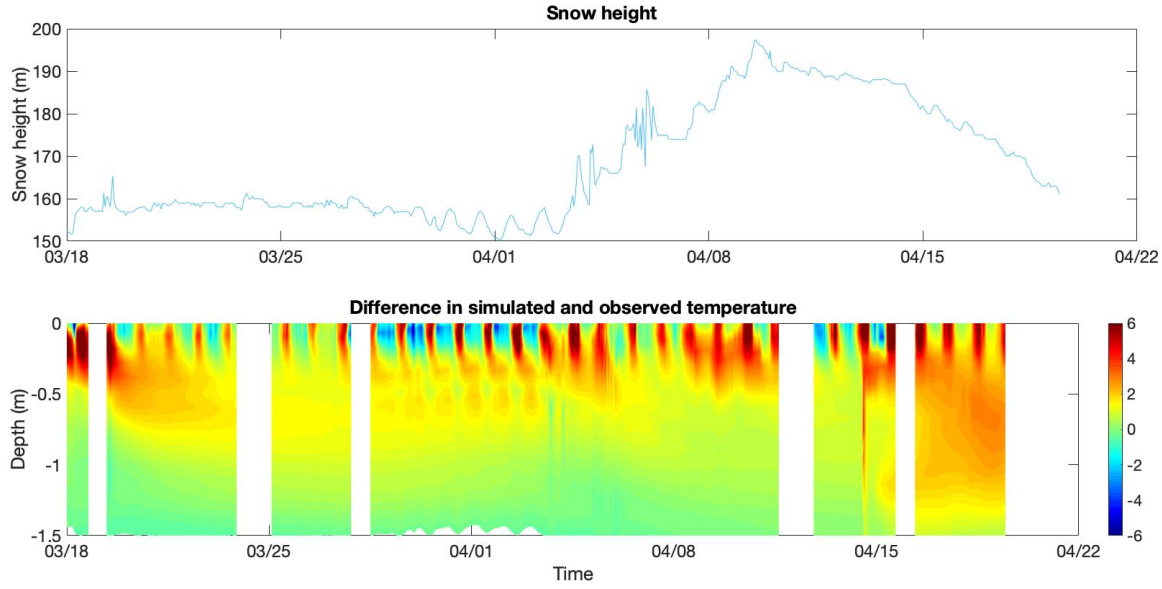

Figure 20: Correlation between strong differences in temperature and snow depth and spikes. The effect seems strongest the days around the 1st of April. Note the slight jump in the time periods.

5.4 Water estimation

The estimation of water content (m_w) is calculated for the whole dataset at once. Marchenko, van Pelt et al. (2018) uses a method where they calculate m_w for each time step. This method should give a more accurate estimation, but as they discuss, the method slightly overestimates the water content. They discuss the overestimation to possibly have several reasons, and mainly that the method attributes the entire misfit between observed and simulated temperature to the effect of refreezing. Other sources of uncertainties can be presence of lateral heat fluxes (the anisotropic effect of k_{eff}) which reduces the validity of the one-dimensional simulations, and uncertainties in the subsurface temperature observations.

The estimation of m_m shows an increase at the 14th of April, which is supported by both the subsurface temperature observations and measurements by the official meteorological station at Finse (figure 21). The air temperature graph (green line) in figure 21 exceeds 0° C the 14th of April, and when considering the surface temperature (purple line) the temperature reaches 0° C for the first time at the same time. During the 16th of April the surface temperature remains at 0° C for the next four days.

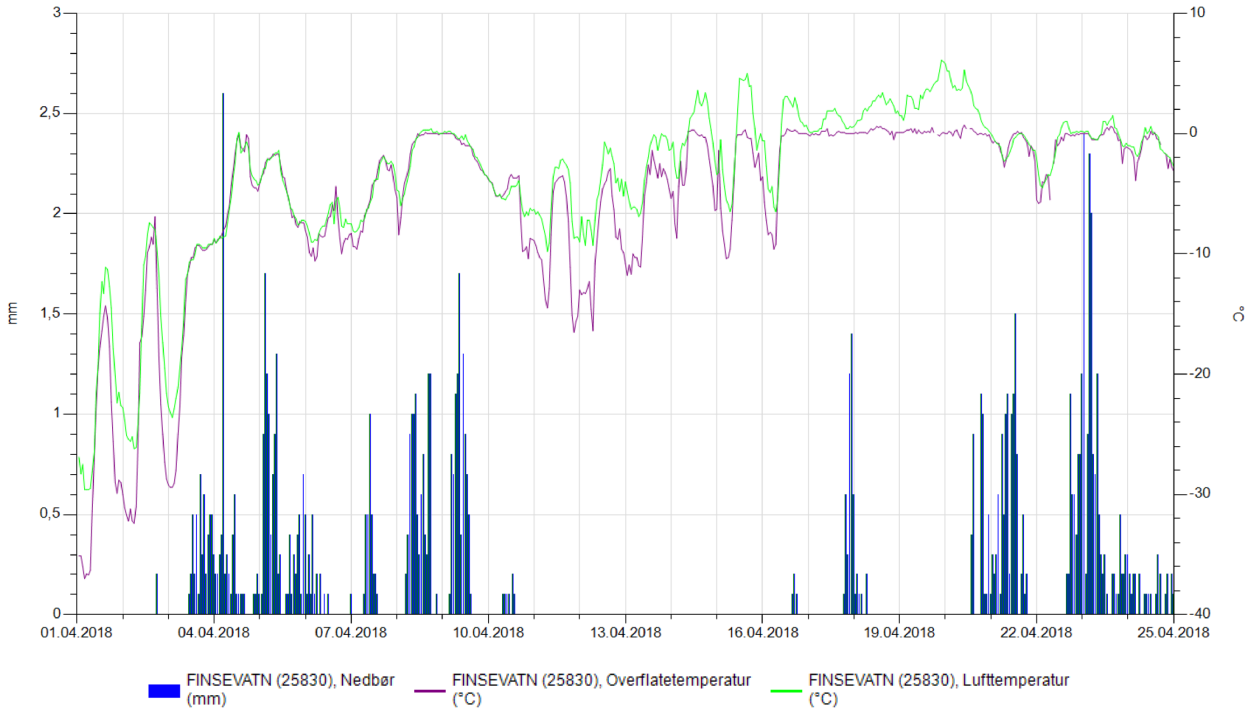

Figure 21: Meteorological data measured by the official met-station at Finse. The blue bars indicate precipitation, the purple line show surface temperature and the green line air temperature (xgeo.no 2019).

The 4th of April, the met-station measures precipitation for a period of six days and during this period the air temperature reaches 0° C at two occasions. When looking at the observed subsurface temperature the same period, there is a warming in the top 0,4 meters and by that some of the precipitation can be assumed to have been rain. If so, this mass of water has not been estimated by the calculation of m_w, which estimates an increase from the 14th when the whole snowpack undergoes a warming towards 0° C. This has justification in the equation estimating the water content (equation 6). The equation subtracts the whole dataset of RC^{meas} from RC^{sim}, and by that does only consider the bulk values. The bulk values will not be able to trace a wetting front as presumably is the case for the mentioned period.

By measuring temperature and run simulations and calculations for several positions, the spatial average result will improve, as in the study by Marchenko, van Pelt et al. (2018) conducted at Lomonosovfonna.

6 Conclusion

The instruments built for this thesis gave promising results and the use of thermistorstrings is a good way to measure snow temperature non-invasive. The input parameters density, effective thermal conductivity and heat capacity were chosen to optimize the model. The model does not include realistic input parameter values, as they are chosen to optimize the simulation in cold snow. The estimation of water content was seen to follow the increased snow temperature. The method works but is considered to have many uncertainties regarding estimation accuracy. Using near infrared photography, a clear correlation between visual observations of the snow layering and NIR images is proven.

6.1 Recommendation for further work

- The temperature simulations and hence the estimation of water content is assumed to have a great benefit of including layering. Dividing the snowpack into sections will presumably allow to trace the wetting process.

- Take measurements of the input parameters at the same spot or within a reasonable distance to minimize the offset in i.e. snow depth at the thermistorstring position.

- Increase number of measurement positions will improve the spatial average result.

7 Literature

References

Armstrong, R. L. and E. Brun (2008). Snow and climate: physical processes, surface energy exchange and modeling, Cambridge University Press.

Avanzi, F., et al. (2016). "Observations of capillary barriers and preferential flow in layered snow during cold laboratory experiments." The Cryosphere **10**(5): 2013-2026.

Barnett, T. P., et al. (2005). "Potential impacts of a warming climate on water availability in snow-dominated regions." Nature **438**(7066): 303.

Brun, E. (1989). "Investigation on wet-snow metamorphism in respect of liquid-water content." Annals of Glaciology **13**: 22-26.

Calonne, N., et al. (2011). "Numerical and experimental investigations of the effective thermal conductivity of snow." Geophysical Research Letters **38**(23).

Colbeck, S. (1982). "An overview of seasonal snow metamorphism." Reviews of Geophysics **20**(1): 45-61.

Colbeck, S. C. (1979). "Water flow through heterogeneous snow." Cold Regions Science and Technology **1**(1): 37-45.

ControlTecnica (2018). "Climatic test chambers." 2019, from https://www.cts-clima.com/en/climatic-testing/climatic-test-chambers.html.

Conway, H. and R. Benedict (1992). Measurements of snow temperature during rain. International Snow Science Workshop (ISSW), ISSW '92 CommBreckenridge, Colo, Citeseer.

Conway, H. and R. Benedict (1994). "Infiltration of water into snow." Water Resources Research **30**(3): 641-649.

DeWalle, D. R. and A. Rango (2008). Principles of snow hydrology, Cambridge University Press.

Domine, F., et al. (2011). "Linking the effective thermal conductivity of snow to its shear strength and density." Journal of Geophysical Research: Earth Surface **116**(F4).

Fierz, C., et al. (2009). TheInternational Classificationi for Seasonal Snow on the Groun, UNESCO/IHP.

Hirashima, H., et al. (2017). "Liquid water infiltration into a layered snowpack: evaluation of a 3-D water transport model with laboratory experiments." Hydrology & Earth System Sciences **21**(11).

Marchenko, S., et al. (2018). Water content of firn at Lomonosovfonna, Svalbard, derived from subsurface measurements. d. o. E. S. University of Uppsala, Uppsala University. **PhD**.

Marsh, P. and M. K. Woo (1984). "Wetting front advance and freezing of meltwater within a snow cover: 1. Observations in the Canadian Arctic." Water Resources Research **20**(12): 1853-1864.

Matzl, M. and M. Schneebeli (2006). "Measuring specific surface area of snow by near-infrared photography." Journal of Glaciology **52**(179): 558-564.

MaximIntegrated (2018). "DS18B20." from https://datasheets.maximintegrated.com/en/ds/DS18B20.pdf.

McClung, D. and P. A. Schaerer (2006). The avalanche handbook, The Mountaineers Books.

Mitterer, C. and J. Schweizer (2013). "Analysis of the snow-atmosphere energy balance during wet-snow instabilities and implications for avalanche prediction." The Cryosphere **7**(1): 205-216.

Riche, F. and M. Schneebeli (2013). "Thermal conductivity of snow measured by three independent methods and anisotropy considerations." The Cryosphere **7**(1): 217-227.

S.L., L. C. D. (2019). Waspmote Datasheet.

Schneebeli, M. (2002). "The importance of the microstructure of snow in nature and engineering." WIT Transactions on Ecology and the Environment **57**.

Sturm, M., et al. (2017). "Water and life from snow: A trillion dollar science question." Water Resources Research **53**(5): 3534-3544.

Sturm, M., et al. (1997). "The thermal conductivity of seasonal snow." Journal of Glaciology **43**(143): 26-41.

Tremper, B. (2008). Staying alive in avalanche terrain, Mountaineers books.

Warren, S. G. (1982). "Optical properties of snow." Reviews of Geophysics **20**(1): 67-89.

xgeo.no (2019). "xgeo.no - graf." Retrieved 29.05, 2019, from http://www.xgeo.no/graphapp/index.html?X=91274&Y=6740808&searchT=10000&stationId=25830.0&app=xgeo.

Yen, Y.-C. (1981). Review of thermal properties of snow, ice and sea ice, Cold Regions Research and Engineering Lab Hanover NH.

Appendix

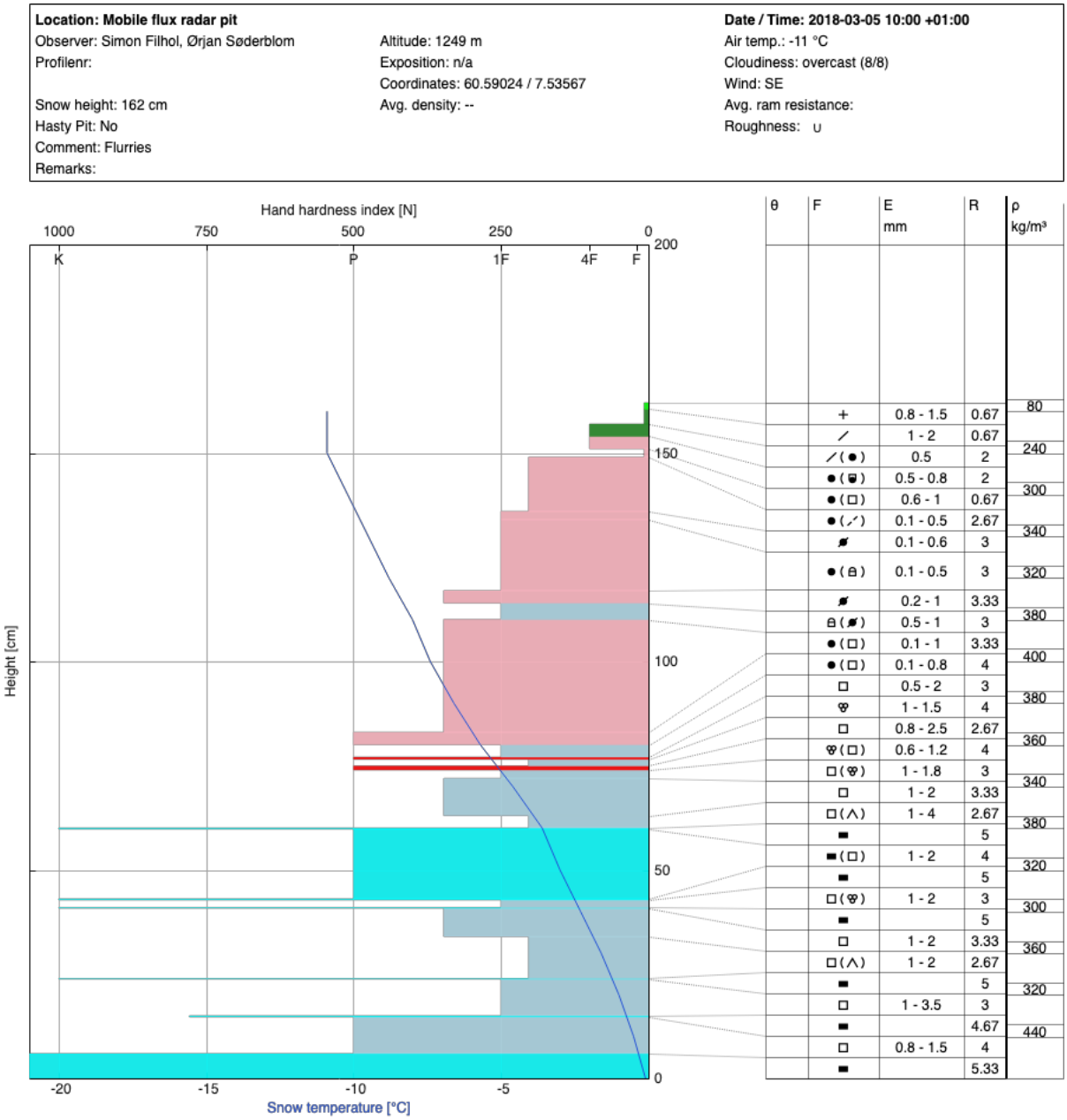

Figure 22: The snow pit data of 05.03.2018.

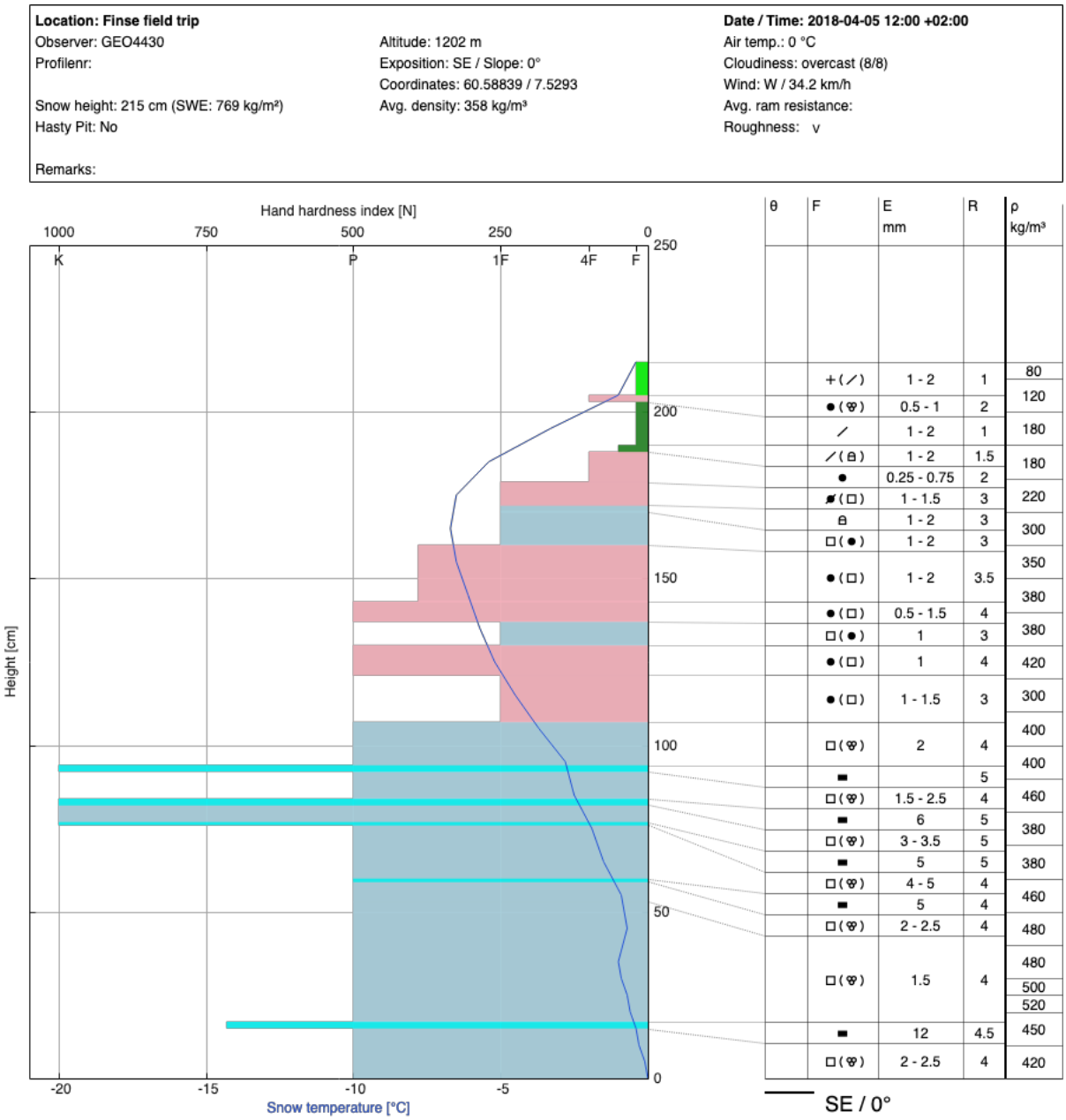

Figure 23: The snow pit data of 05.04.2018.

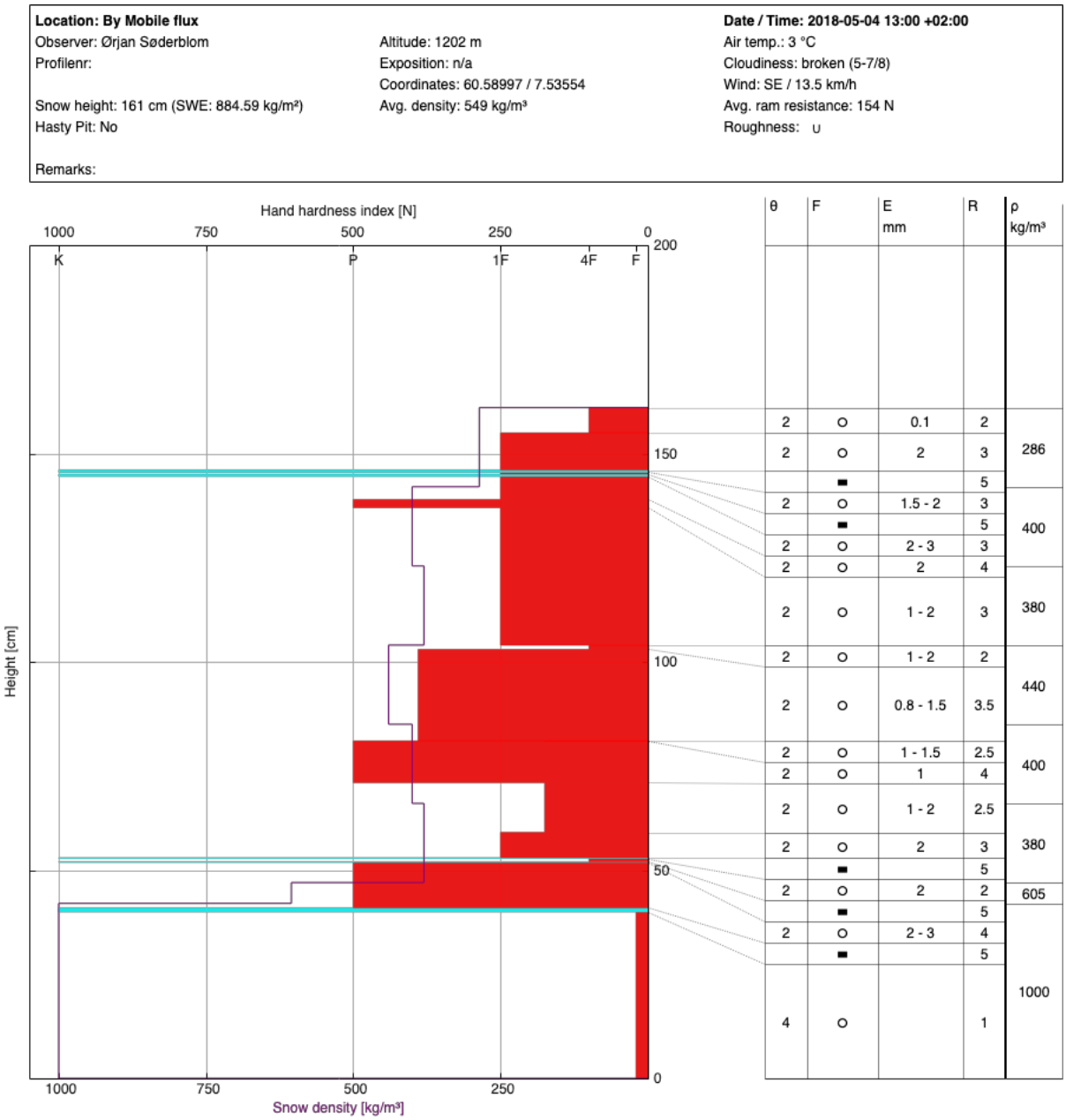

Figure 24: The snow pit data of 04.05.2018.

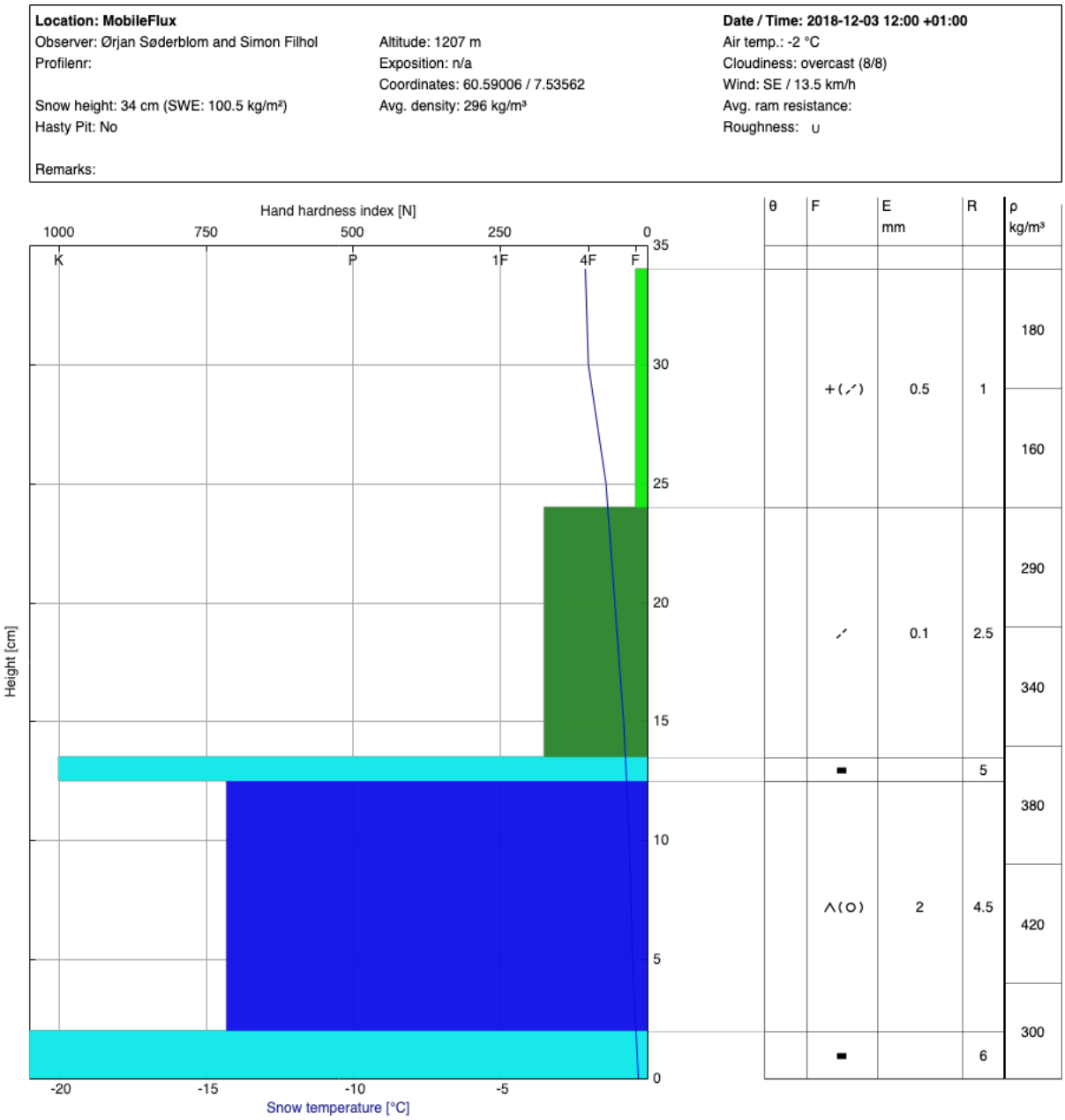

Figure 25: The snow pit data of 03.12.2018.

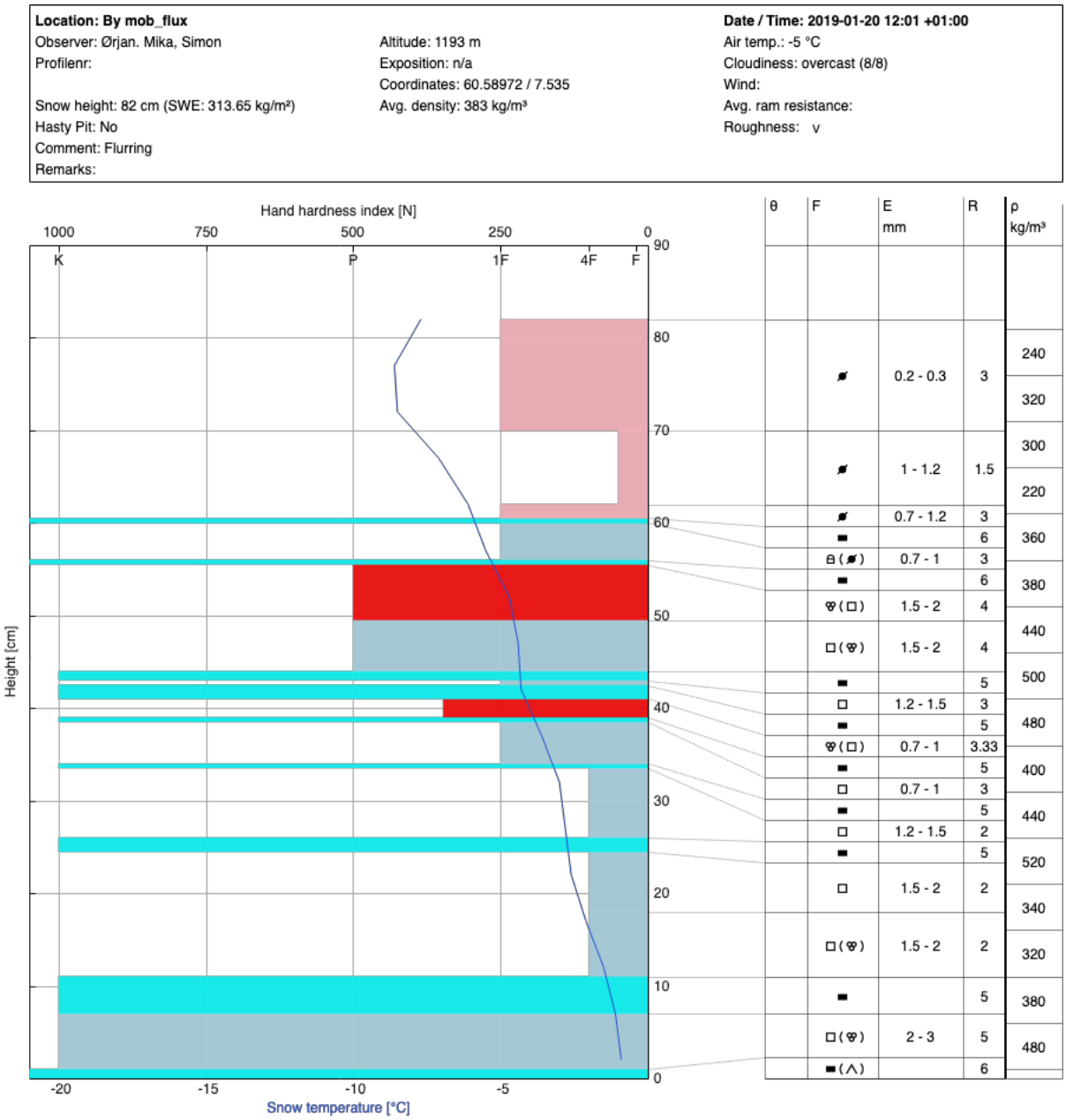

Figure 26: The snow pit data of 20.01.2019.

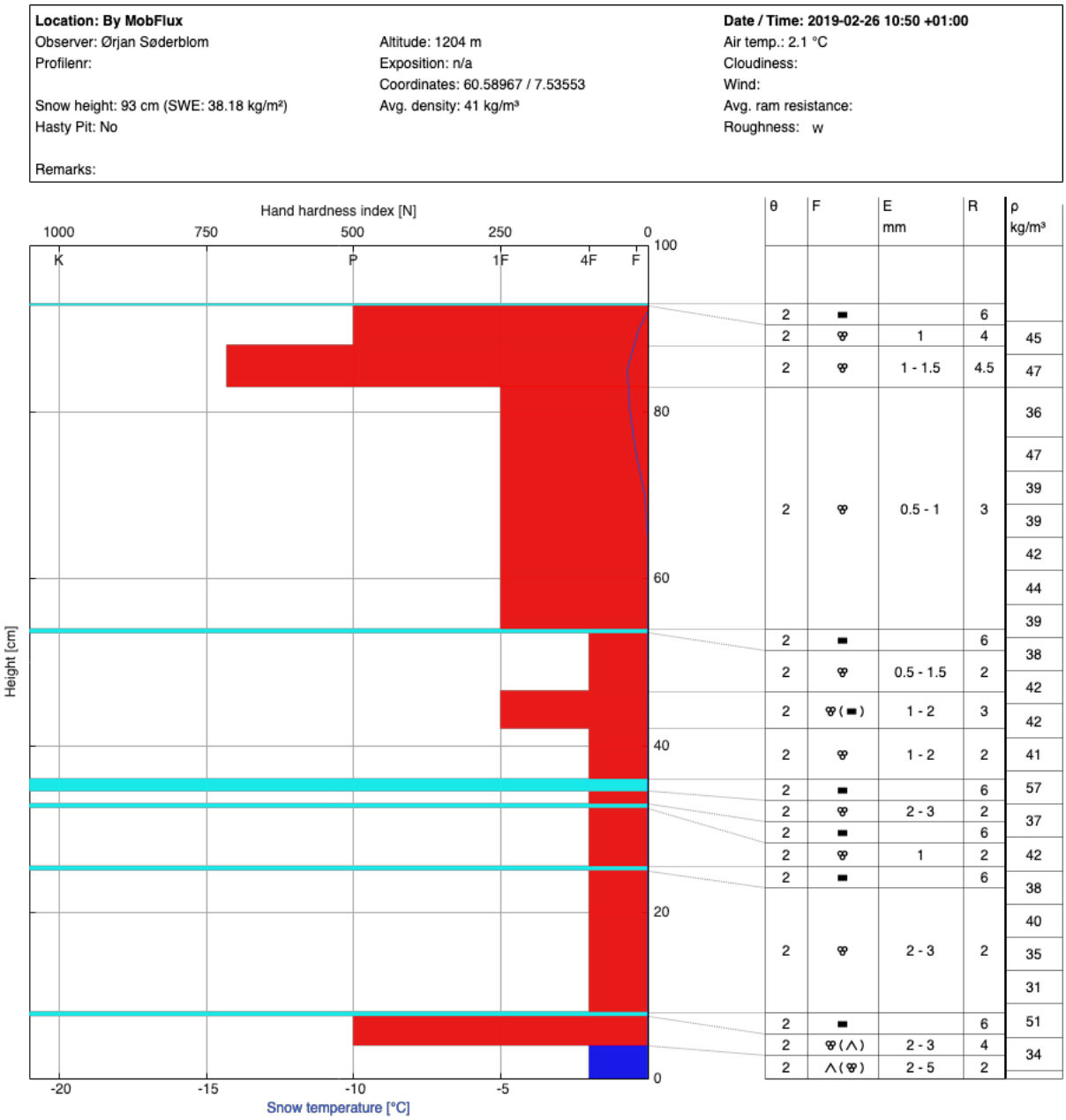

Figure 27: The snow pit data of 26.02.2019.